

Physically-Motivated Modeling of Kinetic Inductance Phonon-Mediated Detector Response for light Dark Matter Searches

Thesis by
Chi Lan Cap

In Partial Fulfillment of the Requirements for the
degree of
Bachelor of Science

The logo for the California Institute of Technology (Caltech), featuring the word "Caltech" in a bold, orange, sans-serif font.

CALIFORNIA INSTITUTE OF TECHNOLOGY
Pasadena, California

2025
Defended May 27, 2025

© 2025

Chi Lan Cap

All rights reserved.

ACKNOWLEDGEMENTS

This thesis project, as well as my understanding of the involved physics, could not have been possible without the incredible mentorship of Professor Sunil R. Golwala, the Golwala group, as well as the KIPM Consortium.

To Professor Golwala, thank you for being an incredibly kind, helpful, and immensely knowledgeable mentor (and classroom professor). I learned the most from our weekly meetings during this project. I am also less afraid of EM these days. To everyone in the group: thank you Brandon and Shilin for being there and for being an example of my future, especially for letting me leak test the fridge once; thank you Robin for your help, reading suggestions, and answering all the questions I have about things I don't understand.

To the KIPM Consortium member, thank you for your helpful and informative feedback, especially at the early stages of this project. Thank you to Dr. Osmond Wen, who is one of my first scientific mentor. I hope I wasn't too rambunctious as a freshman. Thank you Dr. Dylan J. Temples for your mentorship since this summer on all things KIPM-related, getting me started on this project, and providing all of the base coding materials, as well as all the data used here. Special thank yous also to Dr. Yen-Yung Chang, Dr. Taylor Aralis, and Dr. David Moore, whose Ph.D. thesis I consulted, and Dr. Karthik Ramanathan who contributed to the formation of this project.

To Dabney House and the friends we all made along the way: thank you for being my home for the past four years. Nothing I accomplished today would have been possible without this community being the most solid, supportive, and compassionate bedrock of my life. Thank you for mentoring me and allowing me to give back. May the House continue to be what its members need it to be. To my roommates, Jen and Jessie, thank you for walking with me on this conjunction of our dreams. I hope for you two nothing but the most beautiful and meaningful future.

To my family, thank you for trusting me go through this road I chose, even when you do not understand it. My entire life has been founded on your bravery.

Lastly, to the poets and writers, whose steadfast stillness accompanied me through this period of my life; especially Anne Carson, who burst open the door to literature in me. Here is an Anne Carson quote that I reflected on my scientific journey: "If you bring a concept or category up close enough to the human mind to be *very very* attractive and then whisk it away so it stays out of reach, it becomes [flirtatious]... Who would be bothered doing science if it weren't [flirtatious]."

ABSTRACT

The properties of dark matter (DM) is one of the most exciting mysteries in astrophysics, and they are important in understanding cosmological structure formation and could potentially reveal new physics. Direct searches for DM necessitate using ultra-sensitive quantum sensors, one of which is the kinetic inductance phonon-mediated detector (KIPM). Understanding KIPM response is vital to understanding the device's energy resolution. Here, we present a physically-motivated model of KIPM response based on quasiparticle and phonon lifetimes. We examined its adherence to experimental data in three formulations: either six (6τ), five (5τ), or four (4τ) time constants. We examined the temperature-dependence of these time constants, comparing to previous pulse shape models. All three models fit to the data at temperature below 75 mK, with successful fits up to 150 mK in some cases; the 5τ model presented the closest match of temperature-dependence of quasiparticle and phonon lifetimes to existing knowledge, while goodness of fit indicates that 6τ model have the potential to fit high temperature data better. This paper detailed both the behaviors of the physically-motivated models, as well as fitting considerations and the behavior of the fit.

TABLE OF CONTENTS

Acknowledgements	iii
Abstract	iv
Table of Contents	v
List of Illustrations	vi
List of Tables	vii
Chapter I: Motivation and background	1
1.1 Direct detection of dark matter	1
1.2 Kinetic inductance phonon-mediated detectors	1
Chapter II: Characterization of KIPM pulse shape	5
2.1 Empirical model	5
2.2 Convolution model	5
Chapter III: Data overview	9
3.1 Data collection	9
3.2 Quasiparticle lifetime measurement	9
Chapter IV: Procedure for fitting pulse shape	11
4.1 General method	11
4.2 Uncertainty estimation	12
4.3 Fitting behaviors and issues	13
Chapter V: Fitting results	16
5.1 Temperature-dependence of fits	16
5.2 Temperature-dependence of time constants	24
5.3 Amplitude- and Pulse width-dependence of fits	30
Chapter VI: Conclusion	36
6.1 Future work	36
Bibliography	38
Appendix A: Ratio between prompt and delayed amplitude	40

LIST OF ILLUSTRATIONS

<i>Number</i>	<i>Page</i>
1.1 A simple depiction of KIDs mechanism.	2
1.2 Frequency shifts in KIDs	3
2.1 Empirical model fit to data	6
2.2 Temperature-dependence of the delayed and prompt time constants in the empirical model.	7
4.1 The pulse shape at 100.0 mK (left) and 200.0 mK (right) plotted in log-y scale.	12
4.2 6τ fit at 125 mK at $V_{LED} = 3.0V, 4.0V, \text{ and } 5.0V$	15
5.1 4τ fits at 3V, 25 mK, 50 mK, 75 mK, 125 mK	17
5.2 4τ fits of 125 mK at 3V and 4V in two datasets.	18
5.3 4τ fits at 150.0 mK and 175.0 mK, at $V_{LED} = 3.0$ and $4.0V$	20
5.4 4τ fits at 225.0 mK at $V_{LED} = 3.0$ and $4.0V$	21
5.5 The 4τ fit at 300 mK and 325 mK.	22
5.6 Fitting 75 mK pulses with the 5τ and 6τ model.	22
5.7 Fitting 125 mK pulses with the 5τ and 6τ model.	23
5.8 Fitting 220 mK pulses with the 5τ and 6τ model.	23
5.9 4τ fit fall times at 25 mK to 150 mK and 175 mK to 275 mK.	26
5.10 4τ fit quasiparticle lifetime at 25 mK to 150 mK and 175 mK to 275 mK.	27
5.11 5τ fall times and rise time at 25 mK to 150 mK and 175 mK to 275 mK.	29
5.12 The 5τ quasiparticle lifetimes at 25 mK to 150 mK and 175 mK to 275 mK.	30
5.13 The 6τ fall times and rise times at 25 mK to 150 mK, 175 mK and 275 mK.	31
5.14 The 6τ quasiparticle lifetime at 25 mK to 150 mK, 175 mK to 275 mK.	32
5.15 Reduced χ^2 (left, red) versus the starting amplitude	33
5.16 5τ fit at 175 mK and $V_{LED} = 3.0V$, at different starting amplitude.	34
5.17 5τ temperature-dependence of prompt and delayed fall time from 25 mK to 150 mK, at starting amplitude 30%.	35

LIST OF TABLES

<i>Number</i>		<i>Page</i>
5.1	Comparison of prompt t_{fp} and delayed fall time τ_{fd} returned from the convolution models at low temperature.	24
5.2	Comparison of the quasiparticle lifetime τ_{qp} returned from the convolution models at low temperature.	24

Chapter 1

MOTIVATION AND BACKGROUND

1.1 Direct detection of dark matter

Astrophysical (Sofue and Rubin, 2001; Massey, Kitching, and Richard, 2010; Markevitch et al., 2004) and cosmological (Primack, 2017; Aghanim et al., 2020) evidences strongly support the existence of dark matter (DM), a class of massive substances that interact weakly with ordinary matter (see also (Bertone and Hooper, 2018; Strigari, 2013)). Observational evidences has confirmed that DM interacts with ordinary matter via gravity, which was vital to larger structural and galaxy formations. The lack of direct detection evidences, in dedicated searches or in colliders, implies that DM couples very weakly with ordinary matter otherwise. The primary candidates of DM has been Weakly Interacting Massive Particles (WIMPs) at masses around 100 GeV. In addition, there are developments on searches for other non-Standard Model (SM) particles, as WIMPs and these novel particles may reveal new and exciting physics, as well as potentially being able to explain other cosmological mechanisms. In the past decade, the lack of evidence of WIMPs DM has motivated searches for other DM particles. One class of such particles is dubbed *light DM*, where $5 \text{ keV}/c^2 \lesssim m_{DM} \lesssim 500 \text{ MeV}/c^2$.

The couplings of DM to SM particles inform methods in which we can directly detect DM; naturally, the specific couplings involved depend on the DM candidates considered, as detailed in (Sunil R. Golwala and Figueroa-Feliciano, 2022). In particular, the scattering of fermionic DM in the light DM mass range is between the fermionic thermal limit and the lower limit of masses accessible by “nonquantum” techniques. Most of this energy range is below the keV energy resolution in conventional WIMP detection, thus motivating the use of quantum sensors that can detect meV-scale quanta, such as KIPM.

1.2 Kinetic inductance phonon-mediated detectors

Kinetic inductance detectors

A KIPM comprises of a series of kinetic inductance detectors (KIDs) accompanied by a substrate, usually silicon. A KID is a superconducting thin film resonator. Energy depositions (in the form of DM or any interacting particles) shift its resonant frequency and quality factor Q , forming a detectable signal. The advantage of using KIDs lies in the wide options of phonon readout and frequency-multiplexability in the measurement (Temples et al., 2024). In a superconductor, phonon-mediated electrons interactions allow electrons to forms Cooper pairs with $E = 2\Delta \sim \text{meV}$ binding energy. The Cooper pairs carry electrical current without scattering, resulting in

perfect DC conductivity. In an oscillating field, the Cooper pair's inertia causes a delay in their response, thus giving rise to surface impedance on the film. An energy deposition with energy $E \geq 2\Delta$ will break a Cooper pair into a pair of quasiparticles. The decreased Cooper pair density increases the inductive component of the surface impedance, caused by the remaining Cooper pairs speeding up to maintain the same superconducting shielding current derived from the Meissner effect. Meanwhile, the increased quasiparticle density increases the dissipative component of the impedance, thus lowers Q (Sunil R. Golwala and Figueroa-Feliciano, 2022). Fig. 1.1 offers a simple demonstration of how KIDs work, and Fig. 1.2 demonstrates the detected frequency shift.

$$T \sim mK$$

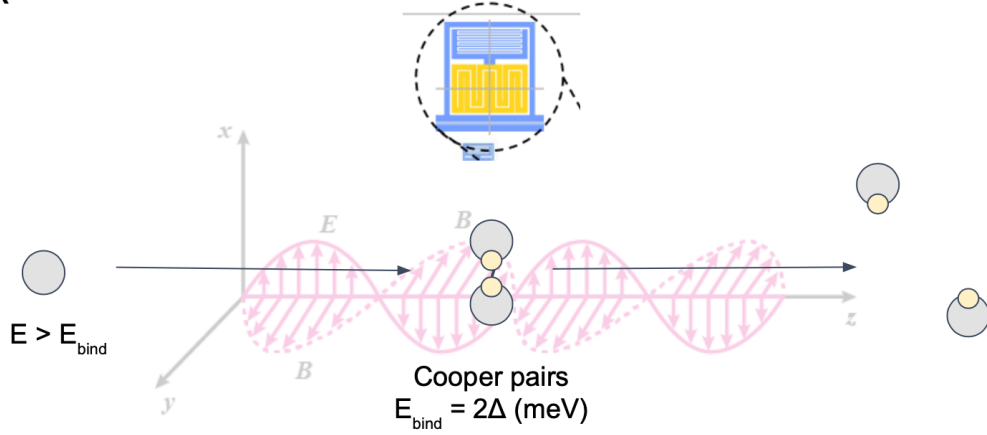


Figure 1.1: On a KIPM, KIDs are maintained at temperature below its critical superconducting temperature $T_c \sim mK$, which allows Cooper pairs to form at $E = 2\Delta \sim \text{meV}$ and give rise to surface impedance in an oscillating field. Incident energy with $E \geq 2\Delta$ breaks a Cooper pair into a pair of quasiparticle. The changes in Cooper pairs density and quasiparticle density shifts the resonant frequency and lowers Q , forming a detectable signal.

Quasiparticle and phonon dynamics in the substrate

In a KIPM, an initial particle - Cooper pair interaction produces a pair of quasiparticles, which then thermalize by producing athermal phonons. On average, most of the excess quasiparticle energy is converted to a single athermal phonon quanta with energy E_{ph} (Hochberg et al., 2016). As the phonon propagates and scatters in the substrate, it can break another Cooper pair and generate more quasiparticles (thus phonons), and it continues to do so as long as $E_{ph} \geq 2\Delta$. This becomes a cascade in the substrate.

The produced quasiparticles also scatters inside the substrate against the crystal N_{surf} times before losing sufficient energy to recombine into Cooper pairs. The quasiparticle lifetime τ_{qp} characterizes this time difference between creation and recombination. We expect τ_{qp} to decrease at high temperature due to the increased thermal quasiparticle density, as $\tau_{qp} \sim (2\Gamma n_{qp})^{-1}$, where Γ is the

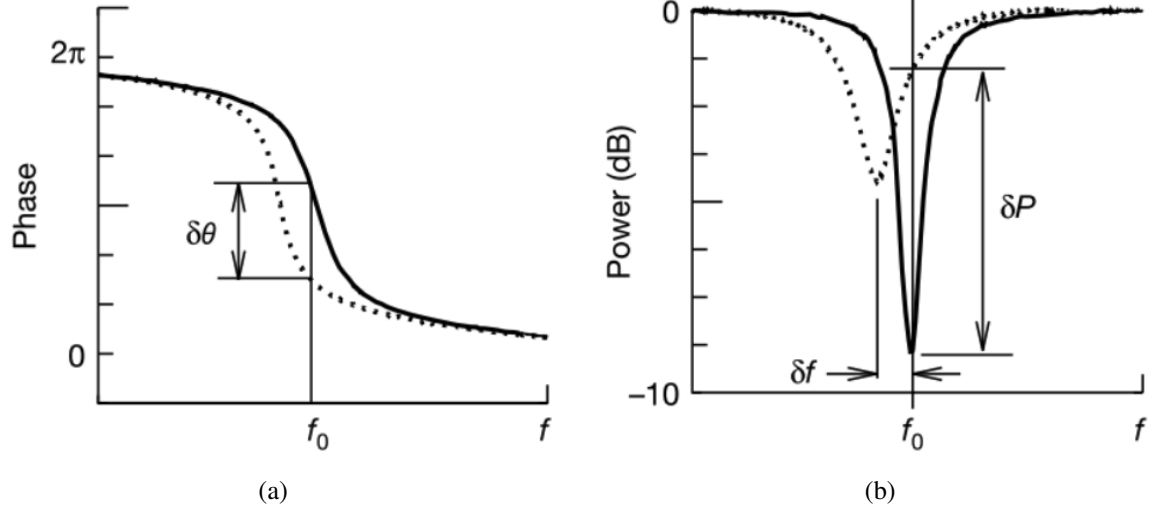


Figure 1.2: The resonant frequency decreased from the quiescent resonant frequency as a result of energy depositions. This manifests as a phase shift at the quiescent resonant frequency in (a), and as a shift in the power spectrum absorption in (b), where the decreased amplitude of the power absorption is due to the lowered Q .

quasiparticle recombination constant and n_{qp} increases as temperature increases (Temples et al., 2024).

We assume the sensor on the surface is only sensitive to phonons above $E_{ph} > E_{min} \approx 2\Delta$, as the lack of electronic states in superconducting band gap prohibits elastic and inelastic scattering of phonon with $E_{ph} < 2\Delta$. This distinguishes athermal from thermal phonons; we are primarily concerned with the athermal population. Following their creations, phonons propagate across the crystal, experiencing isotopic scattering, anharmonic decay, and surface down-conversion. In isotopic scattering, phonons scatter off inhomogeneities in the ion mass; this process is elastic and preserves the phonon spectrum. In anharmonic decay, one phonon decays into two phonons, with lifetime on the scale of 1 s to decay to $E \approx 0.1$ meV (Sunil R. Golwala and Figueroa-Feliciano, 2022). Surface down-conversion is less well understood, but it also limits phonon lifetime. The phonon lifetime represents the characteristic time for phonons in the substrate due to the aforementioned decay processes, as well as due to the loss of energy to sub- 2Δ phonons from various absorption mechanism with surrounding material (Temples et al., 2024). This lifetime yields $N_{surf} > 10^5$, which indicates that surface down-conversion is the dominant thermalization process that creates phonons (Hochberg et al., 2016).

Kinetic inductance phonon-mediated detector

Comprises of the KID layers and the substrate, KIPM detects the incident energy deposition, along with detecting the subsequent phonon and quasiparticles existing in the substrate, thus allowing

for a finer energy resolution and an amplified signal. As phonon and quasiparticles recombine to Cooper pairs, the resonant frequency shifts recovers to the quiescent value in ms timescale.

The Golwala Group at Caltech, and the larger KIPM Consortium, are interested in understanding the behavior of, and developing KIPMs for DM search, which utilizes microwave-KIDs (MKIDs) to detect phonon signals from the device substrate. Formulating an accurate model of KIPM response is vital in understanding the device's energy resolution and sensitivity, where the quasiparticle lifetimes, thus the corresponding quasiparticle density, are necessary in the energy resolution analysis, as further described in (Temples et al., 2024). This project aims to develop a physically-motivated model of KIPM response parameterized by quasiparticle and phonon lifetimes in the substrate, motivated by the current understanding of quasiparticle and phonon behaviors in superconducting crystals.

Chapter 2

CHARACTERIZATION OF KIPM PULSE SHAPE

2.1 Empirical model

Following (Moore, 2012), the KIPM pulse shape has been well-characterized by an empirical model comprises of a fast (prompt) and slow (delayed) component, each component carries two exponential terms for a rise and fall time such that (Temples et al., 2024)

$$\begin{aligned} s_p(t) &= (1 - e^{-(t-t_0)/\kappa_p})e^{-(t-t_0)/\tau_p} \\ s_d(t) &= (1 - e^{-(t-t_0)/\kappa_d})e^{-(t-t_0)/\tau_d} \end{aligned} \quad (2.1)$$

where $\kappa_{p(d)}$ is the prompt (delayed) rise time and $\tau_{p(d)}$ is the prompt (delayed) fall time. The final pulse shape is

$$s(t) = A(s_p(t) + w_d s_d(t)) \quad (2.2)$$

where A is the overall amplitude and w_s is the relative weight of the delayed components.

This model fits to the data at all temperatures, as demonstrated in Fig. 2.1. The prompt and delayed fall time constants decrease monotonically with temperature, as in (Temples et al., 2024) and reproduced here. The maximal amplitude also rises with temperature. Recently, the temperature-dependence of the fall and rise times in (Temples et al., 2024) motivated an interpretation which the fall times in the empirical model represent a time constant that is weakly coupled to temperature (corresponds to an athermal phonon population) and one with stronger dependence (corresponds with the temperature-dependence of n_{qp}), which "switches" role at around 175 mK, as demonstrated in Fig. 2.2.

This model describes the data well, but the physical interpretation of the fall and rise times are not immediately obvious. In addition, since the sensor is only sensitive to quasiparticle response, the quasiparticle and phonon lifetime must be convolved and not trivially separable, as in (Temples et al., 2024). This motivates the physically-motivated convolution models that are the primary focus of this thesis.

2.2 Convolution model

From a phenomenological picture of phonon and quasiparticle dynamics in the substrate, previous works have formulated a differential equation that describe the change in quasiparticle population

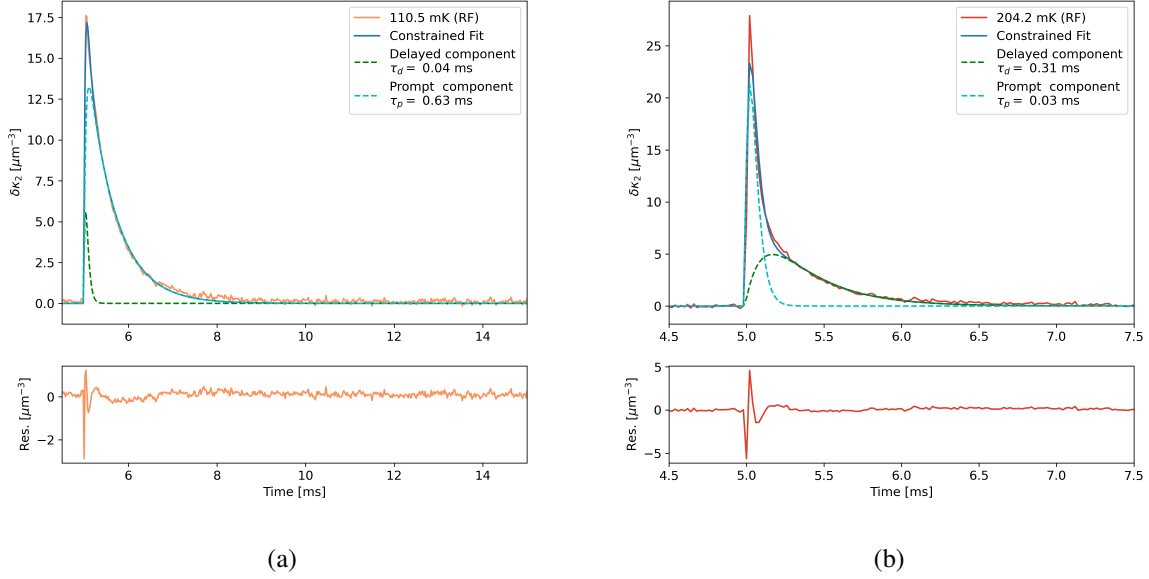


Figure 2.1: at (a) 125 mK, (b) 225 mK. The solid blue line is the overall empirical fit; the dashed green line represented the delayed component and the blue dashed line to the prompt component. The fall time of each component is noted in the legend. The lower panels display the residues of the data, defined to be the difference between the data and the fit.

in time, allowing us to solve for the different time constants involved in forming the detected pulse shape. The derivation is briefly summarized here.

Derivation

Neglecting rise times, assume we have a resonator that satisfies the usual quasiparticle conservation equation

$$\frac{dN_{qp}}{dt} = \eta_{ph} \frac{P(t)}{\Delta} - \frac{N_{qp}}{t_{qp}}$$

where dN_{qp}/dt is the change in quasiparticle density, N_{qp} the quiescent quasiparticle density, t_{qp} the quasiparticle lifetime, η_{ph} is the efficiency of converting absorbed phonons to quasiparticles and $P(t)$ is the phonon pulse from the substrate:

$$P(t) = \frac{E}{N_r} \tau_{abs} e^{-t/\tau_{abs}}$$

where we assumed that the total phonon energy E is split equally among N_r resonators and absorbed over time τ_{abs} . We solve the forced differential equation using Fourier transformations, to yield $N_{qp}(f)$ and its the inverse Fourier transform:

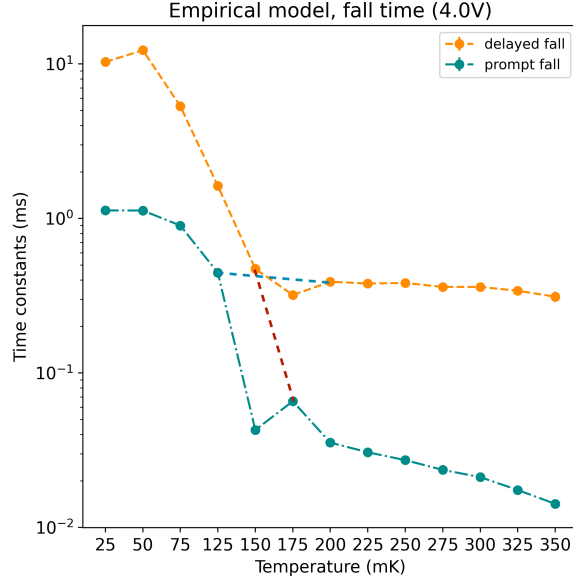


Figure 2.2: This reproduced the results in (Temples et al., 2024). Looking at 150 mK and 175 mK, we can draw a straight line from the plateau of the of the delayed fall line (dashed orange) starting from 175 mK to the prompt fall line (dashed blue) lower than 175 mK, corresponding to a temperature-independent lifetime, as expected for an athermal phonon population. Connecting the delayed fall time below 175 mK to the prompt fall higher than 175 mK, where the tail is still gently decreasing, corresponds to a temperature-dependent lifetime, as expected of a quasiparticle population.

$$N_{qp}(f) = \eta_{ph} \frac{E}{N_r \Delta} \frac{\tau_{qp}}{1 + i\omega\tau_{qp}} \frac{1}{1 + i\omega\tau_{abs}} \quad (2.3)$$

$$N_{qp}(t) = \frac{\eta_{ph} E}{N_r \Delta} \frac{\tau_{qp}}{\tau_{abs} - \tau_{qp}} (e^{-t/\tau_{abs}} - e^{-t/\tau_{qp}}) \quad (2.4)$$

We can generalize 2.3 to attach other time constants into $N_{qp}(f)$ in similar fashions, ultimately yielding

$$\begin{aligned} N_{qp}(t) &= N_{qp}^r \tau_{qp} \int_{-\infty}^{\infty} df e^{i\omega t} \frac{1}{1 + i\omega\tau_{qp}} \frac{1}{1 + i\omega\tau_r} \prod_{\tau_k} \frac{1}{1 + i\omega\tau_k} \\ &= N_{qp}^r \tau_{qp} \left[\frac{e^{-t/\tau_{qp}/\tau_{qp}}}{(\tau_{qp} - \tau_l)(\tau_{qp} - \tau_m) \cdots (\tau_k - \tau_n)} \right. \\ &\quad \left. + \frac{e^{-t/\tau_r/\tau_r}}{(\tau_r - \tau_l)(\tau_r - \tau_m) \cdots (\tau_r - \tau_n)} + \cdots \right] \\ &= N_{qp}^r \tau_{qp} \sum_{\tau_k} \frac{e^{-t/\tau_k/\tau_k}}{(\tau_k - \tau_l)(\tau_k - \tau_m) \cdots (\tau_k - \tau_n)} \end{aligned} \quad (2.5)$$

where $\tau_l, \tau_m, \dots, \tau_n \neq \tau_k$

In general, we expect the phonon interactions to involve a fast (prompt) and slow (delayed) component, each with a rise time (τ_{rp} or τ_{rd}) and a fall time (τ_{fp} or τ_{fd}). This generality take into account quasiparticles that are immediately absorbed by the sensor at their initial collision (prompt) and other which may scatter around the substrates a few times before reaching the sensor, as well as recombination. In the prompt and delayed component, the rise and fall time are convolved with the quasiparticle lifetime τ_{qp} and the resonator ring-down time τ_r , whose values is fixed.

We focuses on the full convolution models (6τ) and two simplified models, where one (5τ) or both (4τ) rise times are assumed to be negligible. Similar to the empirical model, each component has a separate amplitude A_p or A_d , which are symmetrically added to form $N_{qp}(t) = A_p N_{qp,p}(t) + A_d N_{qp,d}(t)$. The 5τ model assumes that the prompt rise time can be ignored, while the 4τ model ignored both prompt and delayed rise time, fitting only for the fall times.

In these models, we bound the time constants to be

$$\tau_{qp}, \tau_{rp} \leq 10 \mu s \quad (2.6)$$

$$10 \mu s \leq \tau_{fp}, \tau_{rd} \leq 1000 \mu s \quad (2.7)$$

$$\tau_{fd} \geq 1000 \mu s \quad (2.8)$$

Chapter 3

DATA OVERVIEW

3.1 Data collection

The data used in this project was collected at the Northwestern EXperimental Underground Site (NEXUS), a low-background cryogenic facility at Fermilab. This data is also used in Temples et al., 2024. The KIPM detector was fabricated at the Jet Propulsion Laboratory and features eleven resonators deposited on a silicon substrate. The primary phonon-absorbing resonator is made of aluminum. The shift in the resonant frequency is measured via the complex transmission

$$S_{21}(f, T) = 1 - \frac{Q}{Q_c} \frac{1}{1 + 2iQ \frac{f - f_r(T)}{f_r(T)}} \quad (3.1)$$

where $f_r(T)$ is the resonant frequency as a function of temperature, Q_c the coupling quality factor, Q is the total quality factor. The shift in the on-resonance transmission δS_{21} in response to change in quasiparticle density δn_{qp} is given by

$$\delta S_{21} = \alpha \frac{Q_r^2}{Q_c} (\kappa_1 + i\kappa_2) \delta n_{qp}(t) \quad (3.2)$$

where t is time, α the kinetic inductance fraction, $\kappa_{1(2)}$ the real (imaginary) component of the fractional change in complex conductivity per unit change in quasiparticle density and has unit of volume.

3.2 Quasiparticle lifetime measurement

The temperature of the mixing chamber (MC) was controlled with a PID-controlled heater, and the MC temperature was swept from 25 mK to 325 mK in steps of 25 mK. We use the LED pulse timestreams, cleaned of correlated noise, from this measurement for our analysis. Once the temperature stabilized, an LED is set to bias at $V_{LED} = 4.0$ or 3.0 , and timestreams were then acquired. The collected data went through a cleaning process and the average pulse is calculated. This average pulse is what is used to fit to a pulse shape model.

Due to the slow thermalization of the RF payloads to the MC, the device temperature is not the same as the MC temperature. A map from MC to device temperature was developed via an auxiliary thermometer installed to the RF payload. The discrepancy increases at higher MC temperature,

leading to increased uncertainty in device temperature. More details are discussed in Temples et al., 2024.

In later analysis, we refer to each dataset by their MC temperature (25 mK to 325 mK), whereas the graphs presented labeled the data by their RF temperature.

Chapter 4

PROCEDURE FOR FITTING PULSE SHAPE

4.1 General method

We perform the fits using the Python `iminuit.py` package. In this use case, `iminuit` is more robust than the typically-used `scipy.curve_fit` package, as the latter tends to fail and return no parameters for higher temperature data. The package requires the y-axis uncertainty, as well as initial guesses of the fit parameters. In addition, we rely on the in-house `KIPD_Analysis` package for several helpers functions, such as estimating the initial guesses and other graphic-related task.

Using the `iminuit`'s built-in least square cost function, we use the `MIGRAD` and `HESSE` functions provided to minimize the cost function and to calculate uncertainty, respectively. References for `iminuit` is available at Hans Dembinski, 2022. Each fit returns the fitted parameters, the corresponding errors, and several indicators of goodness of fit. These include the reduced χ^2 value, `iminuit`'s internal "estimate distance from minimum" (EDM) value, which it uses to judges the validity of the fit (by being below a certain EDM threshold). We primarily use the reduced χ^2 value to evaluate the goodness of fit. In addition, we rely on visually inspecting the fit when necessary.

To obtain the initial guesses required by `iminuit`, we estimated the pulse shape as a single exponential line to obtain the location and value of the amplitude. Next, since the convolution form is in the exponential form e^{-t/τ_k} , we obtain estimates of fall time constants τ_k 's from the different segments of linear slopes in the logarithmic form of the pulse. Fig. 4.1 demonstrates the linear slopes for two cases: one at low temperature with two fall times, the other at high temperature with three. We assume the fastest timescale, i.e, that with the steepest slope, is τ_{qp} . The second- and least-steep slopes are ascribed to τ_{fd} and τ_{fp} respectively. This step is not currently automated and requires by-hand inspections.

To ensure proper fitting, we discard a portion of the beginning and of the end of the data. Initially, we discarded and began the fit after the pulse has fallen to around 80% of its amplitude. We excluded data points beyond 15 ms, after sufficient time that the pulse settled to about $0.0 \mu m^{-3}$. Pruning the beginning and end in this manner also ensure uniformity between the quality of fits between different temperature and guiding the fit to focus on the downward slope instead of the peak. We observed that while starting at later time (at lower amplitude) may benefits fitting (see Sec. 4.3 and Sec. 5.3), cutting more of the tail does not improve the fit. Excluding the earlier time in the pulse may have an experimental motivation as well: these early time features non-linear behaviors, where there are additional noise from readout probes and the reflection of sine waves from the readout.

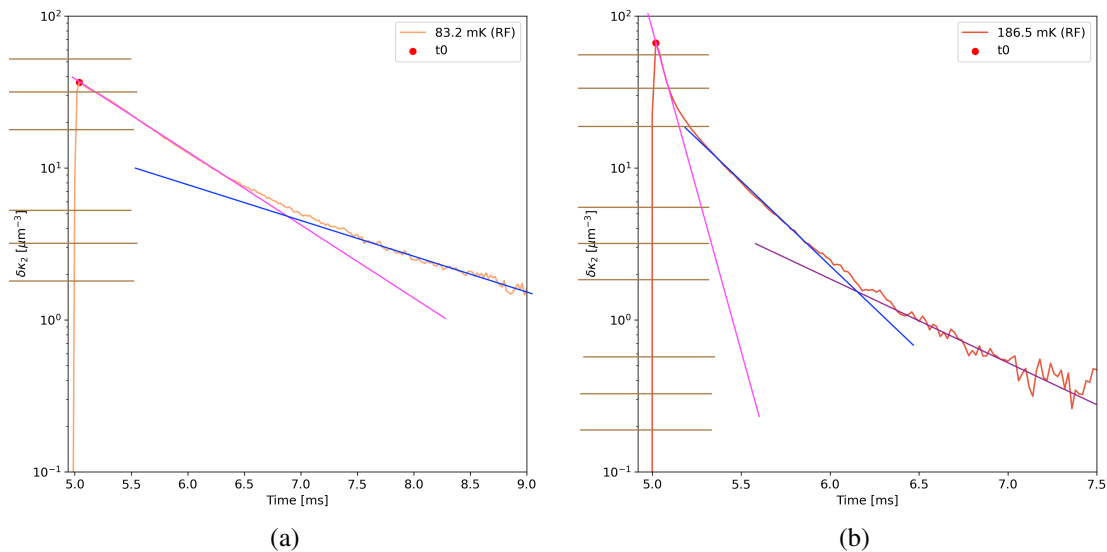


Figure 4.1: The pulse shape at 100.0 mK (left) and 200.0 mK (right) plotted in log-y scale. In this scale, we can see the different segments of linear slopes that corresponds to a different time constant τ_k in e^{-t/τ_k} . These slopes are used as the initial guesses for `iminuit` to perform the fit. The brown lines on the y-axis (unfortunately no longer erasable) assists in determining the y-value at different points.

This ring-down period (corresponds to τ_r is also not well understood. We nonetheless included τ_r in the fit as a fixed values for accuracy. Experimentally, τ_r may be longer. Excluding the early time thus simplifies the fitting process.

We provide the fits with bounds of the floating time constants, aforementioned in 2.6. We also place the additional constraints that $A_p > 0$ and $A_d > 0$.

Inputting this information to `iminuit` will begin the fitting process. From the returned parameters and reduced χ^2 value, we calculated also the ratio between the amplitude of the prompt and delayed component, $\alpha_{pd} = A_d/A_p$. We graphed the fit on top of the pulse and saved the returned parameters and goodness-of-fits information in a `.txt` file. The graph of each fit is accompanied by a graph of its residue, defined as the difference between the data and the fit for the entire length of the data, including points that are not included in the fit.

4.2 Uncertainty estimation

We estimated the uncertainty in the average pulse from the power spectral density (PSD) of the signal. We assume that the frequency noise is white, where the power spectral density (PSD) $J(f)$ is constant. The integral of the noise PSD gives the noise variance in time. Obtaining the uncertainty from frequency space also have the benefits that, for linear systems, the behaviors at each frequency are independent of each other (Sunil R Golwala, 2000). Thus we get the time variance

$$\sigma^2 = \sum_i J(f_i) df$$

where df is the frequency bin width of the PSD. We divide σ^2 by N , the number of pulses used to calculate the final average pulse. The final uncertainty is taken to be $\delta = \sqrt{\sigma^2/N}$.

4.3 Fitting behaviors and issues

The fitting process is refined over this thesis project as we experiment with different models and ways to implement them. Below are some significant challenges to the fitting process and any modifications that has been made, outside of the general fitting method.

Variables degeneracy

In writing the convolution models in the form of Eq. 2.5, we observed that the fitting programs cannot effectively differentiate between the time constants, even with constraints, due to the symmetric roles they play in the equation (i.e., τ_{qp} could easily be τ_{fd} or any other time constants, in the eyes of the fitting function). The empirical model avoided this issues since each exponential term carries a unique combination of time constants. We follow that form and rewrite the prompt component of the 6τ model:

$$\begin{aligned}
N_{qp,p}(t) = & A_p \frac{e^{-t/\tau_{qp}}}{(\tau_{qp} - \tau_{fp})(\tau_{qp} - \tau_r)(\tau_{qp} - \tau_{rp})} \\
& \times \left[1 - e^{-t/\tau_r} \frac{\tau_{qp} (\tau_{qp} - \tau_{abs})(\tau_{qp} - \tau_{rse})}{\tau_r (\tau_r - \tau_{abs})(\tau_r - \tau_{rse})} \right. \\
& \times \left[1 - e^{-t/\tau_{abs}} \frac{\tau_r (\tau_r - \tau_{qp})(\tau_r - \tau_{rse})}{\tau_{abs} (\tau_{abs} - \tau_{qp})(\tau_{abs} - \tau_{rse})} \right. \\
& \left. \left. \times \left(1 - e^{-t/\tau_{rse}} \frac{\tau_{abs} (\tau_{abs} - \tau_{qp})(\tau_{abs} - \tau_r)}{\tau_{rse} (\tau_{rse} - \tau_{qp})(\tau_{rse} - \tau_r)} \right) \right] \right] \quad (4.1)
\end{aligned}$$

where

$$\begin{aligned}
\frac{1}{\tau_{rse'}} & \equiv \frac{1}{\tau_{rse}} - \frac{1}{\tau_{abs}} \\
\frac{1}{\tau_{abs'}} & \equiv \frac{1}{\tau_{abs}} - \frac{1}{\tau_r} \\
\frac{1}{\tau_r'} & \equiv \frac{1}{\tau_r} - \frac{1}{\tau_{qp}}
\end{aligned}$$

The final model will be of the form

$$N_{qp}(t) = A_p N_{qp,p} + A_d N_{qp,d}$$

The 5τ and 4τ models are similar constructed, with the modifications that each component in the 4τ form will only have three time constants. The 5τ form thus will have a three- and a four-time constants term. We show here the form for a three- time constants term as appears in 4τ :

$$N_{qp,3\tau} = A \frac{e^{-t/\tau_{qp}}}{(\tau_{qp} - \tau_{abs})(\tau_{qp} - \tau_r)} \left[1 - e^{-t/\tau_r} \frac{\tau_{qp} (\tau_{qp} - \tau_{abs})}{\tau_r (\tau_r - \tau_{abs})} \right. \\ \left. \times \left(1 - e^{-t/\tau_{abs'}} \frac{\tau_r (\tau_r - \tau_{qp})}{\tau_{abs} (\tau_{abs} - \tau_{qp})} \right) \right] \quad (4.2)$$

where

$$\frac{1}{\tau_{abs'}} \equiv \frac{1}{\tau_{abs}} - \frac{1}{\tau_r} \\ \frac{1}{\tau_r'} \equiv \frac{1}{\tau_r} - \frac{1}{\tau_{qp}}$$

High amplitude pulses

Fitting data on different V_{LED} setting reveals that at the same temperature, the width of the pulse is largely the same, but there is a substantial difference in the pulse amplitude. The same temperature in 4.0V data has an amplitude about two to three times higher than that of 3.0V. As the temperature increases, the pulse amplitude increases as well, which may contribute to the difficulty in fitting higher temperature curves. Figure 4.2 demonstrates the difference of a 6τ fit at 125 mK with V_{LED} 3.0V, 4.0V, and 5.0V. This widening of the fitted curve for higher amplitudes also warns that data with high and narrow pulses, such as that at higher temperature, will be more difficult to fit accurately, if at all.

If the fitting quality depends on the amplitude, given that we are primarily interested in the fall times rather than rise times, we are motivated to prune more of the peak for a better fit. This change could be physically motivated. The convolution models is derived assuming $\delta n_{qp} \ll n_{qp,0}$, where $n_{qp,0}$ is the quiescent quasiparticle density. We know that $n_{qp,0} \approx 20\mu m^{-3}$ at low temperature, though it may be higher as temperature increases. Thus, we only need to care about the portion of the pulse from such amplitude downwards. Through experimentation with starting the fit at different amplitudes (parameterized as percentage of the true peak) we decided to fit up to 50% or 80% of the pulse for lower temperature (25 mK to 125 mK) and 30% of the pulse for higher temperature (125 mK to 350 mK) for the temperature-dependence analysis in Sec. 5.2. We discuss the results of this variation in Sec. 5.3.

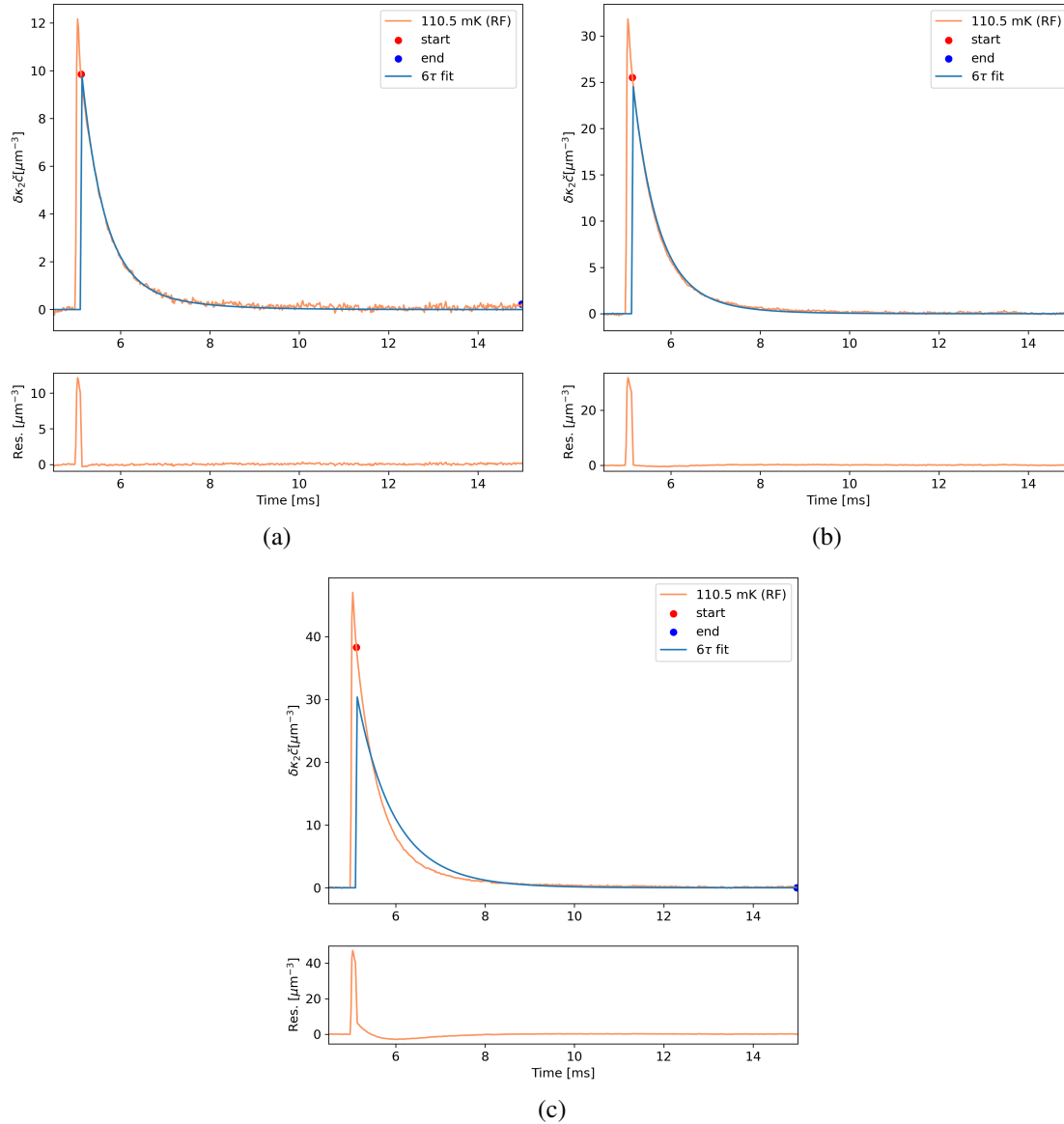


Figure 4.2: 6τ fit at 125 mK at $V_{LED} =$ (a) 3.0V , (b) 4.0V, and (c) 5.0V. The width of the data pulses are approximately equal, but the fitting function failed at fitting the pulses with higher amplitudes. In (b) the fit subtly overshoot the downward curve starting at 6 ms, whereas in (c) the fit overestimated the width of the curve completely.

Chapter 5

FITTING RESULTS

We review the results of the three convolution models across temperature, intensity of the source V_{LED} for the two datasets available, 0215 and 0216, commenting primarily on the quality of the returned fits. We begin by discussing the variation of fit behaviors and qualities in Sec. 5.1 using the 4τ model as the simplest model, then comparing it to the 5τ and 6τ models. Sec. 5.3 discusses the effect of pulse amplitude on fitting capabilities by examining data at different V_{LED} s settings, also starting with 4τ fit. Sec. 5.2 compares the three models in greater details by examining the temperature-dependence of the time constants as returned by the fit. In addition, as noted in Sec. 3, we refer to the temperature by the setpoint temperature MC, while in-graph labels reference the RF temperature of the data.

5.1 Temperature-dependence of fits

In this analysis we focus on the 0216, $V_{LED} = 3.0V$ dataset, with comparisons to any $V_{LED} = 4.0V$ and 0215 data as necessary. We retained 80% of the amplitude for all temperature here for uniformity.

General temperature-dependence behavior: 4τ

At all V_{LED} , the 4τ model is a good fit at low temperature, with reduced $\chi^2 \approx 1.0$ at 75 mK and below. At $V_{LED} = 3.0V$, as shown in Fig. 5.1, reduced χ^2 may fall below 1.0, leading to risk of overfitting. Nonetheless, the residuals indicate that 4τ model returns random residuals that are near zero, indicating that the fit matches to the data. At 125 mK, reduced $\chi^2 = 3.60$, though as shown in Fig. 5.1 the model still fits with low residuals. Possibly, the higher scaling of the data "inflates" the reduced χ^2 value. The same can be seen when comparing the 125 mK of the two datasets in Fig. 5.2 (top). The amplitude of the pulse is the primary difference in the data and the fit, since the width of the pulses does not vary with temperature. Here, the reduced χ^2 value of the lower-amplitude data is also lower. At this amplitude, $\delta n_{qp} \lesssim n_{qp,0}$, well within the constraint assumption of the exponential models, thus the pulse fits well to the exponential shape and easily matches the amplitude of the data given to the fit.

Starting from 150 mK, the fits begin to depart from the curve, beginning to become more pronounced at 175 mK where the amplitude of fits fall below the starting amplitude. The differences in fit qualities from 125 mK to 175 mK are more pronounced at higher voltage settings, as shown in Fig. 5.3. In addition, at 150 mK, the tail starting at 7 ms subtly undershoots the real data. The

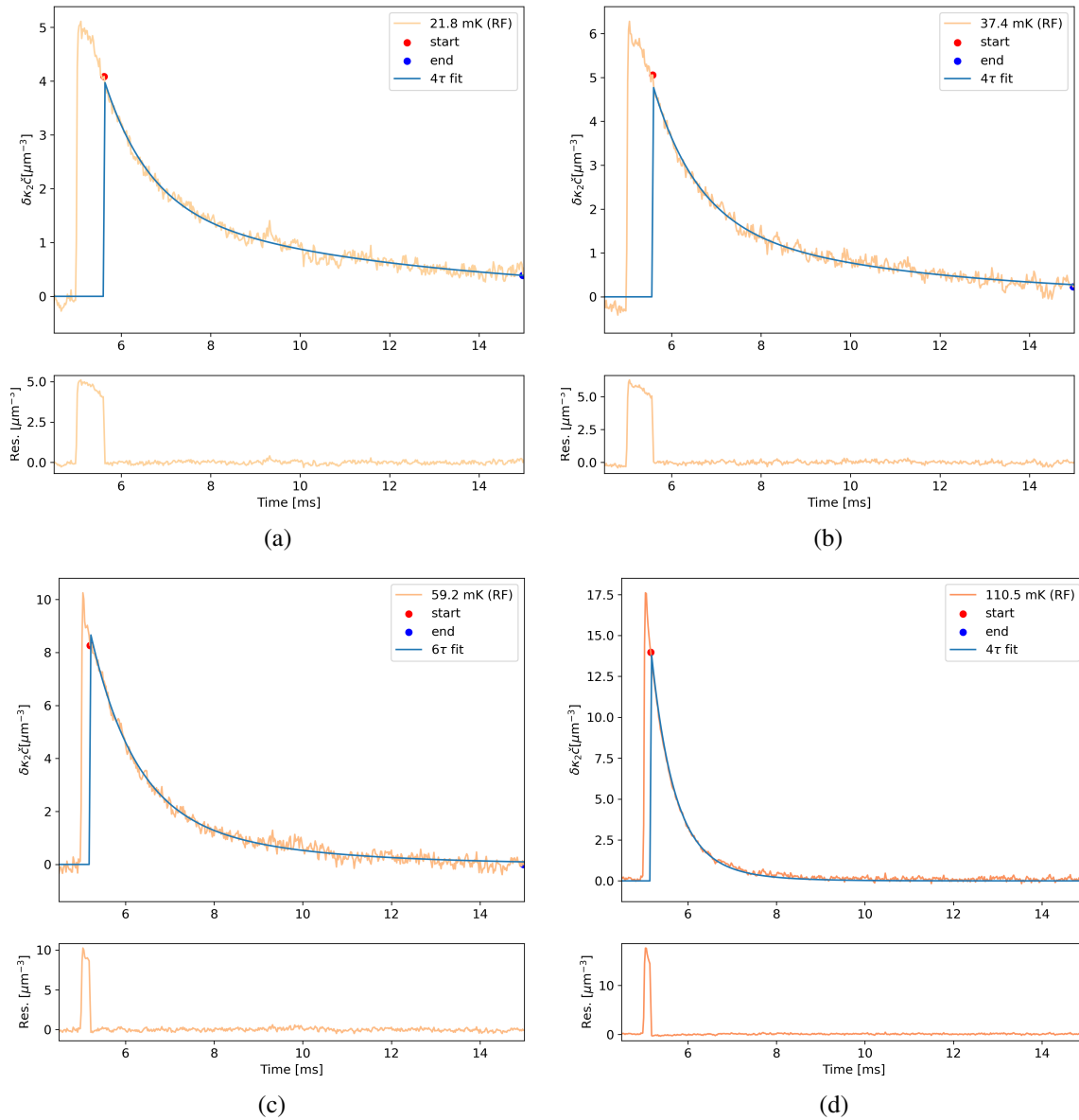


Figure 5.1: 4τ fits at 3V, (a) 25 mK; (b) 50 mK; (c) 75 mK; (d) 125 mK. The 4τ model fits well at this regime of low temperature, with reduced $\chi^2 = 1.06$ at 25 mK, reduced $\chi^2 = 0.89$ at 50 mK, reduced $\chi^2 = 0.76$ at 75 mK, and reduced $\chi^2 = 3.60$ at 125 mK. We noted that reduced $\chi^2 < 1.0$ may indicates over-fitting. The bottom portion of both graphs display the residue of the fit. In both all fits, starting from the fit begins at before 6 ms, the residue is approximately 0, indicating a good match between the data and the fit.

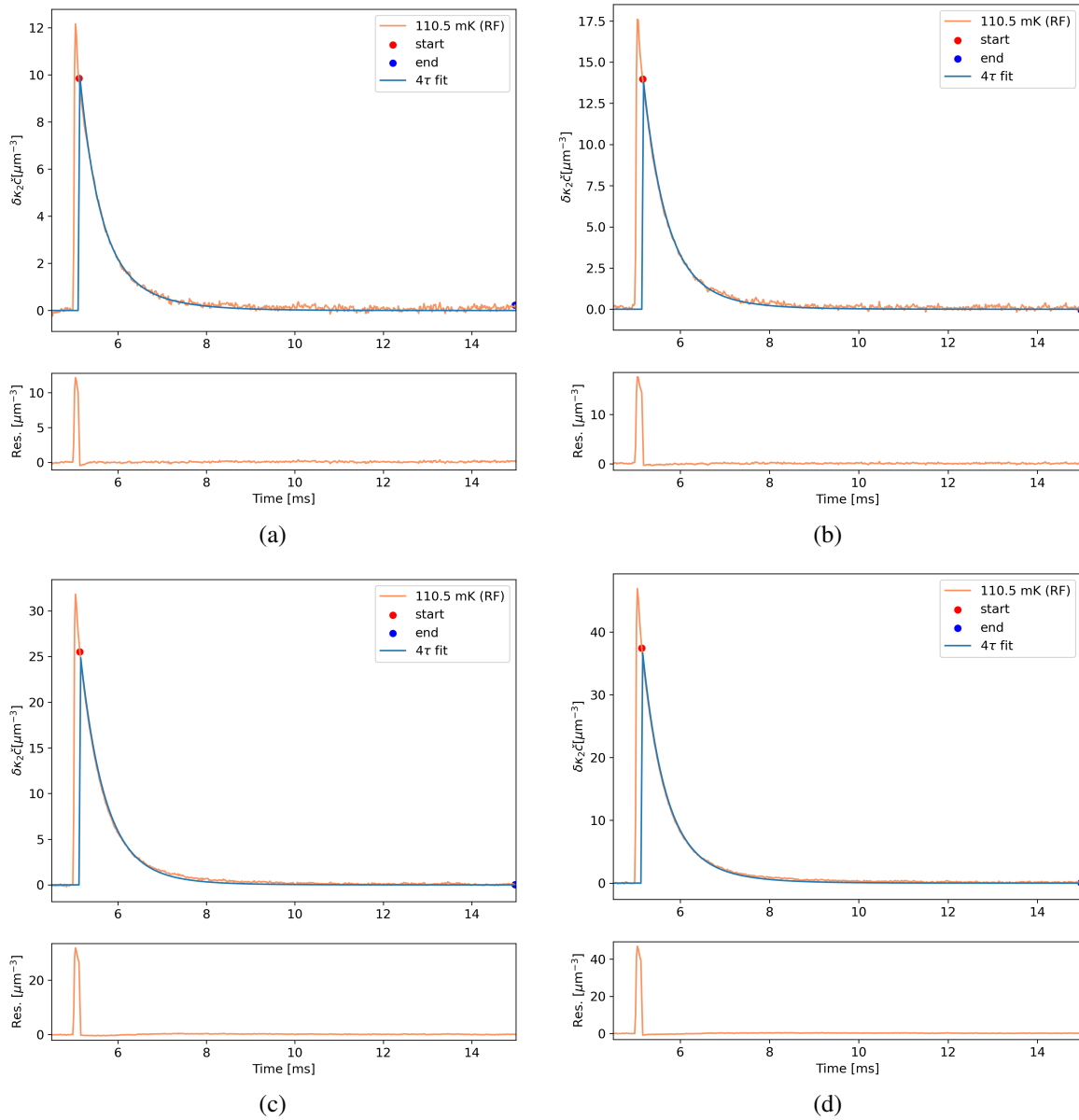


Figure 5.2: 4τ fits of 125 mK at *Top*: 3V, (a) 0215 dataset, (b) 0216 dataset. The 0216 datasets have higher amplitudes, which fits to a narrower pulse as seen in the residue around the pulse spike (5 ms). *Bottom*: 4V, (c) 0215 dataset, (d) 0216 dataset. At higher voltage, we begin to see some deviation from the curve at around 7 ms, where the fitted curve did not decay fast enough.

undershoot in particular is unique to 125 mK and 150 mK, thus is likely to be an artifact of the fits rather than anything physical. Most importantly, at around 6 ms (Fig. 5.3, (b)) we begin to see the fitted pulse becoming wider than the data curvature. This is exacerbated in the 175 mK fits. It takes increasingly longer for the fits to re-converge with the data at higher temperature. A wider curve means the fitted fall times are overestimated here. The reduced $\chi^2 \gg 1$ here (Fig. 5.3 (d)) showed that this is not a good fit. Starting at these temperature, the narrowing of the pulse in addition to the steeper amplitude makes it more difficult for the fits to find the minimum. From 175 mK, reduced $\chi^2 \gtrsim 26$.

The fit becomes highly unreliable and not well-explained starting from 225 mK. As shown in Fig. 5.4 (a), the width of the fit is much larger than that of the data. Notably, in (b), though the amplitude of the data is much higher for the same width, the fit's width is much narrower. Comparing the 125 mK to 175 mK fitted curve with the 225 mK curve in (a) shows that they have approximately similar width; here, the fit failed to "narrow" itself in accordance to the actual curve, though (b) demonstrates that it might be possible for the fit to adapt. As later shown in 5.3, shifting the fitting range to lower amplitudes help with fitting the later-time curve, in some cases by forcing the fitted curve to narrow.

At 300 mK and higher, the pulses narrow further in addition to having higher amplitudes. The value of successive data points fluctuates more compare to lower temperature, which may reflects a more complex and/or active quasiparticles propagation and recombination in the substrates. Reduced $\chi^2 \sim 1.0$ at 325 mK and 350 mK, though in general, the fits are very unpredictable in these regimes and returns parameters with uncertainty much larger than the scale of the time constants. In Fig. 5.5, comparing the fits in (a) and (b), the better fits start at a lower starting point and the better fit only fits to the less-steep tail end of the pulse from approximately 5.1 ms onwards. On the logarithmic scale, as in Fig. 4.1, this part of the curve corresponds to the phonon fall times that dominates after the very rapid quasiparticle lifetime fall off. Though the residuals are better compare to, say, 275 mK or 350 mK, the time constants returned does not make physical sense nor match well with what is predicted by examining the graphs, and with very high error bars. Thus, we still consider the fits to be unreliable at high temperature.

Later on, we noted, but has not extensively investigated, how starting the fit at lower amplitudes improve the fits at higher temperature in Sec. 5.2.

Comparison to 5τ and 6τ models

Similar to the 4τ fits, the 5τ models fit the low temperature well, similarly with reduced $\chi^2 \sim 1.0$ below 75 mK and reduced $\chi^2 = 2.11$ at 125 mK, jumping to reduced $\chi^2 \gg 1$ at higher temperatures, starting at 150 mK. Notably, the width of the fit begins to deviate from the curve at 150 mK or

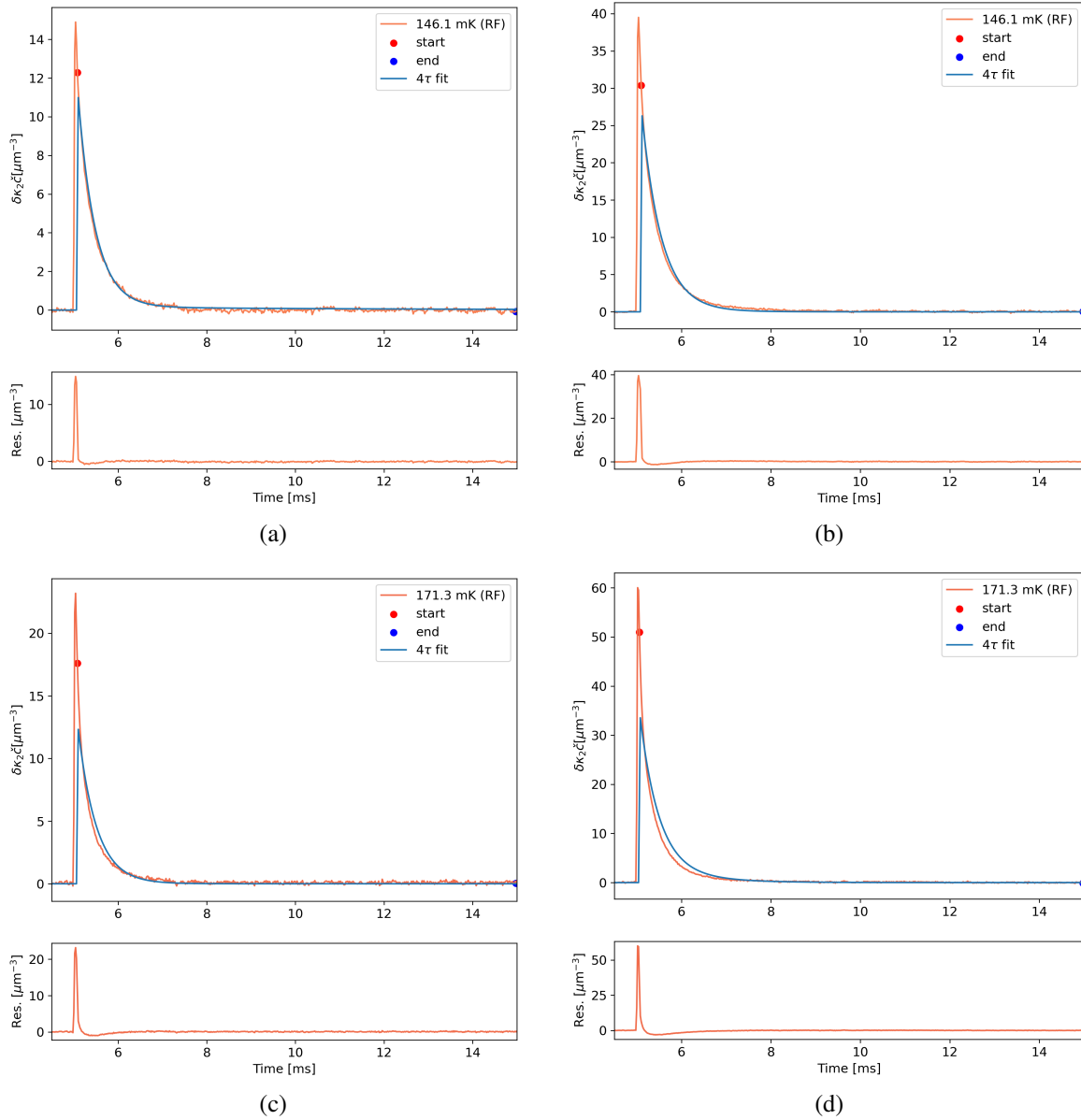


Figure 5.3: 4 τ fits at *Top*: 150 mK fits at (a) 3.0V, (b) 4.0 V. *Bottom*: 175 mK fits at (c) 3.0V, (d) 4.0 V. Deviation from the width of the pulse begins to appear at these temperature. The narrower pulse shape is more difficult to fit. At higher voltage, we begin to see some deviation from the curve at around 7 ms, where the fitted curve did not decay fast enough.

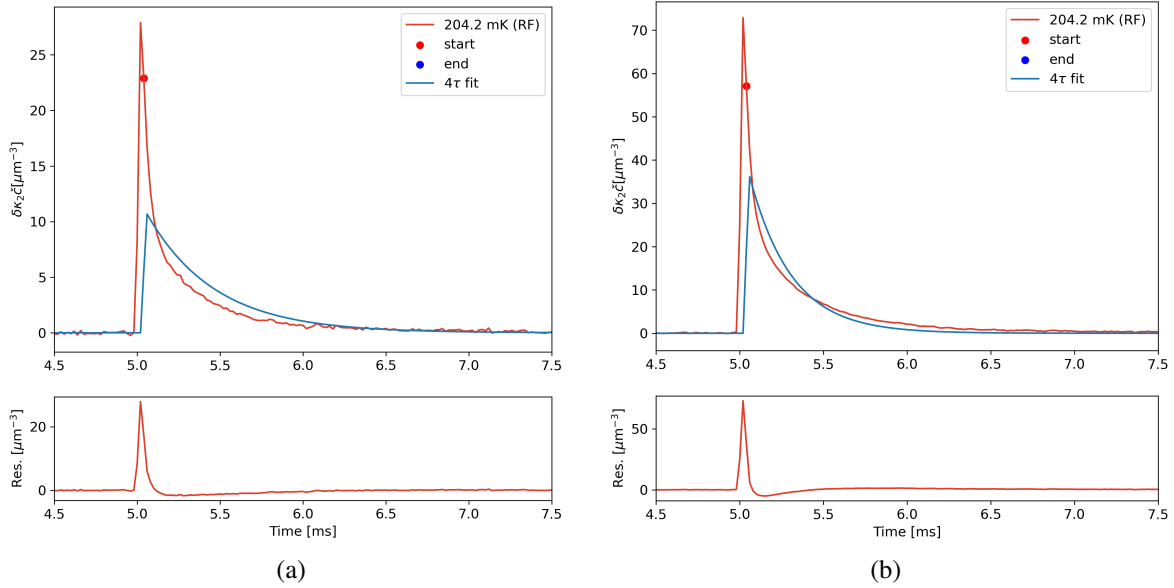


Figure 5.4: 4τ fits at 225 mK fits at V_{LED} (a) 3V; 4V. At 225 mK the fits begin to fail to narrow up to the curve, with some exceptions. Note the restricted range of the displayed graph at these temperature (up to 7.5 ms instead of 15.0 ms like before), such that the same pulse width, as in (a), now looks wider compares to curves at lower temperatures.

175 mK occasionally, depending on the dataset used. This problem appears consistently from 200 mK, a little earlier than in 4τ for the same datasets. Physically, this is reasonable to expect, since the delayed rise time matter less at low temperature and this parameter is primarily associated with recombination rate. Specifically, at higher temperature, phenomena like recombination become more dominant due to higher energy phonons being emitted, where $E_{ph} > E_{band}$, the latter being the band gap of the substrate. Higher recombination rates means phonon returns to the sensor at sufficiently high energy, contributing to the delayed fall time τ_{fd} and possibly the delayed rise time τ_{rd} as well.

The same temperature-dependent is seen in the 6τ fit. This may be a sign that the rise times are negligible, particularly the prompt rise time. However, the fit at higher temperature, though still not accurate, are more viable in the 6τ models than other models, as demonstrated in Fig. 5.8. There may be a complex interface between the importance of the rise time as temperature increases, as the prompt rise times are still small in 6τ even at higher amplitude.

At lower temperature, the delayed fall times returned by 5τ are within 10% to 15% of what is returned by 4τ , while the prompt fall times discrepancies are 30% or over 70%, as shown in Table. 5.1. The large discrepancy in parameters is surprising consider the great fits in these temperatures; evidently, the returned time constants depends strongly on the models being used. Due to the fit starting at a later time, it is possible that the prompt fall time is not fully captured by the fit, thus resulting in

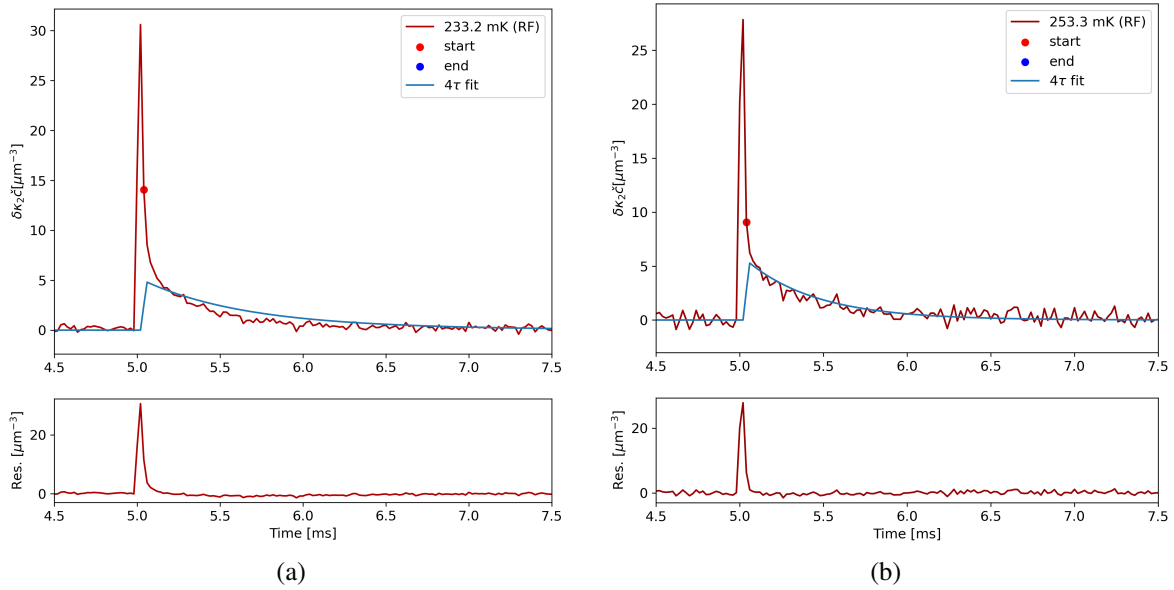


Figure 5.5: The 4τ fit at (a) 300 mK; (b) 325 mK. At higher temperature, the fitting function cannot fit up to the amplitude and instead focuses on the downward slope (which is, fortunately, of main physics interest). The fits at these temperatures are highly unpredictable and sensitive to small changes made to the fitting procedure. We often exclude data at these temperature in our discussion due to their unpredictability.

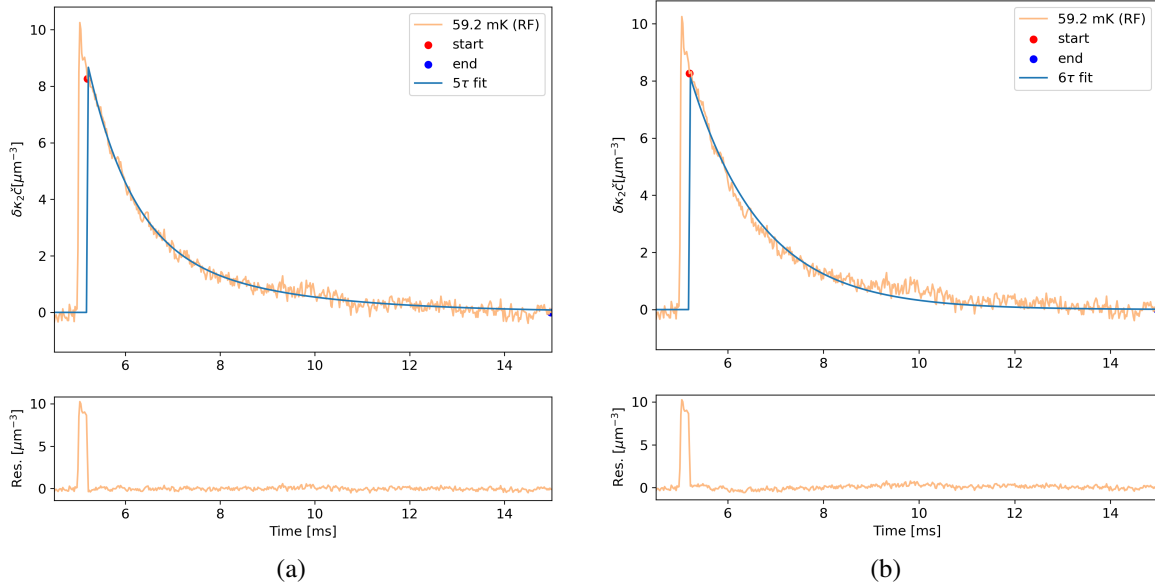


Figure 5.6: Fitting 75 mK pulses with the 5τ and 6τ model. At low temperatures, the 5τ model (a) matches well with the data pulse, with residues randomly fluctuate around 0 after the beginning of the fit at 5 ms. In (b), the 6τ curve generally fits well but with a slower decreasing slope from 6 ms to 8 ms, with the fit slightly underestimate the curve before 6 ms and overestimate it after 6 ms.

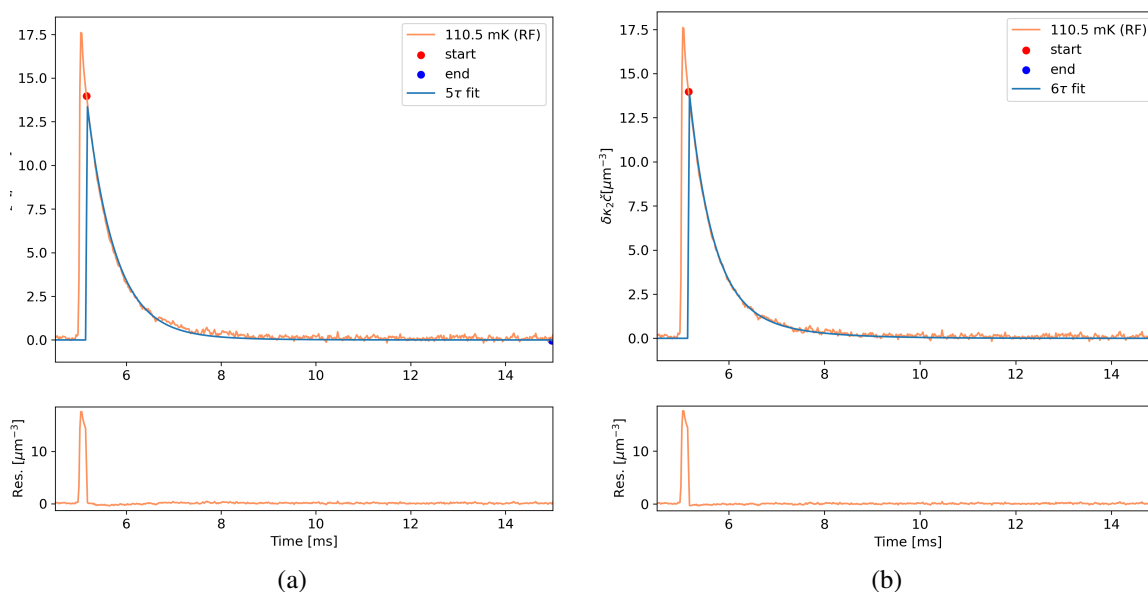


Figure 5.7: Fitting 125 mK pulses with the 5 τ and 6 τ model. At this temperature, 6 τ in (b) fits the curve well, with residues randomly fluctuate around 0 after the beginning of the fit at 5 ms. The 5 τ fit in (a) underestimated the curve slightly at around 7 ms.

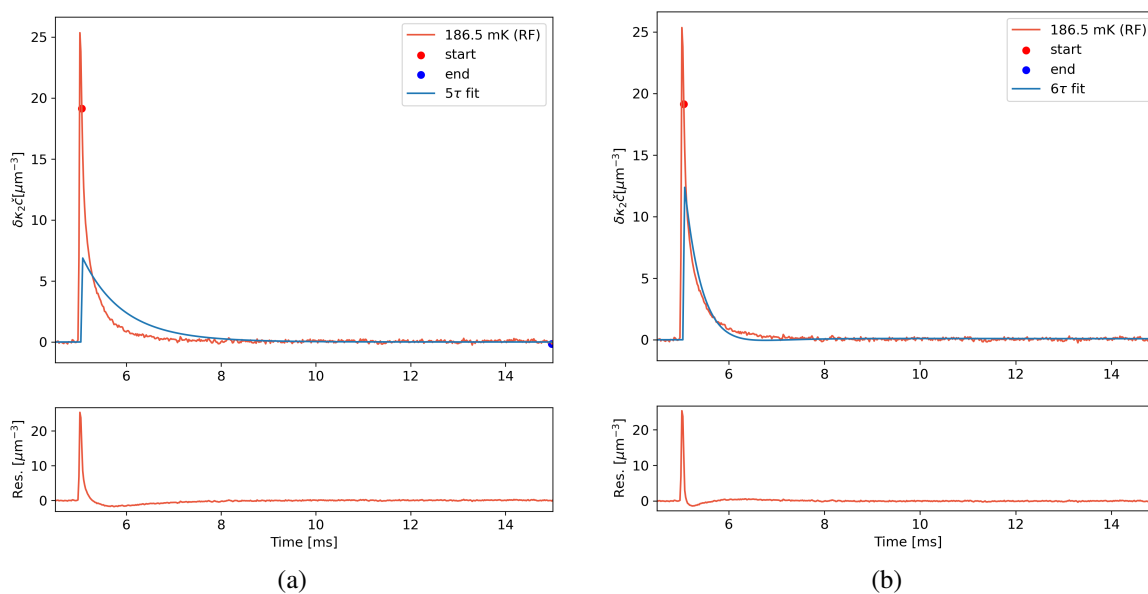


Figure 5.8: Fitting 220 mK pulses with the 5 τ and 6 τ model. Starting from this temperature, the fits tend to fail, most commonly by overestimating the curve width as in (a). The 6 τ fit in (b), while still not a good fit, is able to overcome that challenge and offers a better match to the curve.

higher discrepancies between the models despite the good fit returned. The discrepancies also grows as temperature grows, potentially reflecting the temperature-dependence of the time constants and of phonon interactions, such as recombination. The quasiparticles lifetime τ_{qp} have more dramatic, but consistent, differences between the models, where the parameter returned by 5τ and 6τ matches about two-times better than either matches to 4τ (Table 5.2). Disagreements between 4τ and 6τ are especially dramatic, which is expected as they are the most different from one another. It is thus surprising to see that the `iminuit` fitting (via the returned χ^2 value) "believes" that 4τ and 6τ matches the data best, and less so for 5τ . In our case, the reduced χ^2 might not have been the most rigorous judge of fit-ability.

	25 mK		50 mK		75 mK	
	τ_{fd}	τ_{fp}	τ_{fd}	τ_{fp}	τ_{fd}	τ_{fp}
4τ	6.4 ± 0.3	1.0 ± 0.7	5.1 ± 0.2	1.0 ± 0.03	3.1 ± 0.2	0.97 ± 0.05
5τ	6.7 ± 0.1	0.3 ± 0.02	4.2 ± 0.1	0.2 ± 0.1	2.8 ± 0.2	0.67 ± 0.07
6τ	5.7 ± 0.9	0.04 ± 0.03	1.0 ± 0.03	0.3 ± 0.02	1.0 ± 1.2	0.2 ± 0.02
$\delta_{4,5\tau}$ (%)	4.1	70	17	77	11	31
$\delta_{4,6\tau}$ (%)	11	96	78	69	68	78
$\delta_{5,6\tau}$ (%)	16	689	282	25.8	175	213

Table 5.1: Comparison of prompt t_{fp} and delayed fall time τ_{fd} returned from the convolution models at low temperature. At 25 mK to 75 mK, the fits are most successful. We compare the discrepancy between each model by its fractional difference, represented here as a percentage, where $\delta_{m,k} = |\tau_m - \tau_k|/\tau_k$

	τ_{qp}		
	25 mK	50 mK	75 mK
4τ	0.4 ± 0.1	0.34 ± 0.03	0.3 ± 0.01
5τ	1.3 ± 0.02	0.72 ± 0.02	0.8 ± 0.07
6τ	1.9 ± 0.3	1.1 ± 0.03	1.5 ± 0.02
$\delta_{4,5\tau}$ (%)	70	52	56
$\delta_{4,6\tau}$ (%)	79	69	78
$\delta_{5,6\tau}$ (%)	30	35	40

Table 5.2: Comparison of the quasiparticle lifetime τ_{qp} returned from the convolution models at low temperature. At 25 mK to 75 mK, the fits are most successful. We compare the discrepancy between each model by its fractional difference, represented here as a percentage, where $\delta_{m,k} = |\tau_m - \tau_k|/\tau_k$

5.2 Temperature-dependence of time constants

Here we evaluate the temperature-dependence of the phonon and quasiparticle lifetime constants in different models. For each temperature, we evaluate the low temperature regime (25 mK to 150 mK) and the high temperature regime (175 mK to 275 mK) separately first, then consider them together. The 300 mK and up data is excluded due to the overall instability and high uncertainty of

the fits. We compare the temperature dependence of these models to that of the empirical model in Fig. 2.2, which has been shown to fit well to the data. In this section we use data from both 0215 and 0216, selecting the V_{LED} dataset that shows more insight into the fit's behaviors.

We are motivated to choose a different starting amplitude for the low temperature (25 mK to 150 mK) and high temperature (150 mK to 275 mK) regime. The amplitude chosen is parameterized as the percentage of the true amplitude of the data. Practically, we choose to start the fit at the data point closest to this chosen amplitude value; at higher temperature, due to its very steep descend at earlier time, the percentage may not accurately reflect where the fit begins. Further details and motivation is discussed in Sec. 5.3.

- 4τ ($V_{LED} = 3.0$ V), low T: 80%
- 4τ ($V_{LED} = 3.0$ V), high T: 30%
- 5τ ($V_{LED} = 3.0$ V), low T: 50%
- 5τ ($V_{LED} = 3.0$ V), high T: 50%
- 6τ ($V_{LED} = 4.0$ V), low T: 50%
- 6τ ($V_{LED} = 4.0$ V), high T: 30%

From Fig. 2.2, we expect the prompt and delayed fall times to decrease with increasing temperature, before the delayed fall time flats out at 175 mK, and the prompt fall time decreased more slowly after 175 mK.

4 τ model

Using $V_{LED} = 3.0$ V, the delayed fall time in the 4τ model suggestively follows the trend observed in the empirical model, excluding the outlier point at 150 mK (Fig. 5.9). The prompt fall time stays constant from 25 mK to 75 mK, then falls steeply from 75 mK to 125 mK and falls more gradually at 150 mK, suggesting a rougher, but still similar, trend in the empirical model (where the steepness of the decrease is from 75 mK to 150 mK). The high temperature data from 175 mK also shows the same stagnancy of the prompt fall time as in the empirical model, with a deviation at 225 mK that is the outlier temperature of all fall time fits. However, all the delayed fall time in the 0216 data has very high uncertainty. For the prompt time fall, after 175 mK they fall flat instead of decreasing further. Following the empirical model's interpretation of the "switch" in roles of prompt and delayed fall time in Sec. 2.1 and in Temples et al., 2024, where the delayed fall time corresponds to a thermal population below 125 mK and the prompt fall time corresponds to

an athermal one at the same range, before switching at 125 mK, we observe that same transition at 75 mK. In Fig. 5.9 (a), we can draw a straight line connecting the prompt (light blue) line from 75 mK to the fall (orange) line, with both datasets 0215, 0216 agreeing. The temperature dependency does not hold at higher temperature. In total, the 4τ model at $V_{LED} = 3.0V$ roughly replicate the trend shown in the empirical model. The same result is not replicated $V_{LED} = 4.0V$, which is of note because the latter is the voltage used to produce the empirical model's time-dependence here.

The discrepancy from the overall trend at 225 mK is potentially due to the degeneracy between the prompt and fall component. With the reformation of the model in Sec. 4.3, we resolved the degeneracy between quasiparticle lifetime τ_{qp} , phonon fall time $\tau_{fd(p)}$ and rise time $\tau_{rd(p)}$ (where applies). Since the prompt and delayed components are added symmetrically, there may be unresolved degeneracy between τ_{fd} and τ_{fp} . We can see this trend of the delayed and prompt fall time complementing each other at 225 mK, 250 mK, and 275 mK in 0215 data (brown and dark blue line). The jump in the delayed fall time of 0216 at 225 mK may suggest the same degeneracy, though the prompt fall time for the same data set does not reflect this possibility.

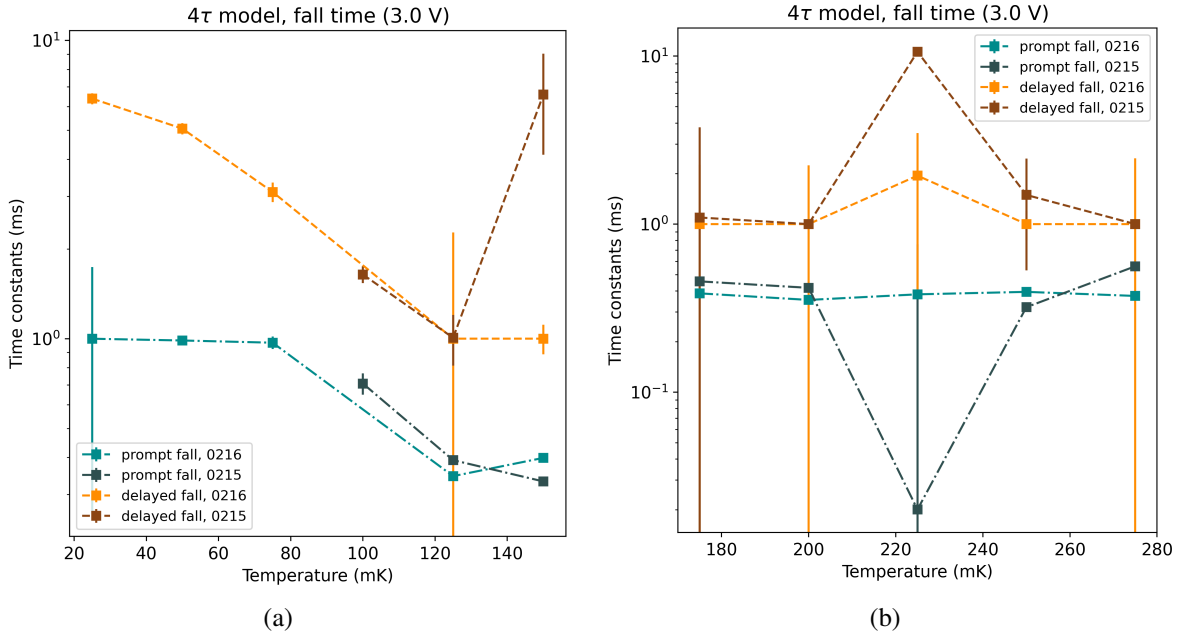


Figure 5.9: The 4τ fit fall times at (a) 25 mK to 150 mK and (b) 175 mK to 275 mK. The temperature dependence of the prompt and delayed fall time in (a) reflects the expected trend coming from the empirical model. At higher temperature, degeneracies of the fall times might arise, causing discrepancy to the expected trend. We see the transition of prompt and delayed fall time being thermal and athermal, respectively, switched at 75 mK, as suggested in the empirical model.

The quasiparticle lifetime τ_{qp} , as shown in Fig. 5.10, follows the same trend where it decreases with temperature from 25 mK to 75 mK. As aforementioned, τ_{qp} grows shorter at higher temperature

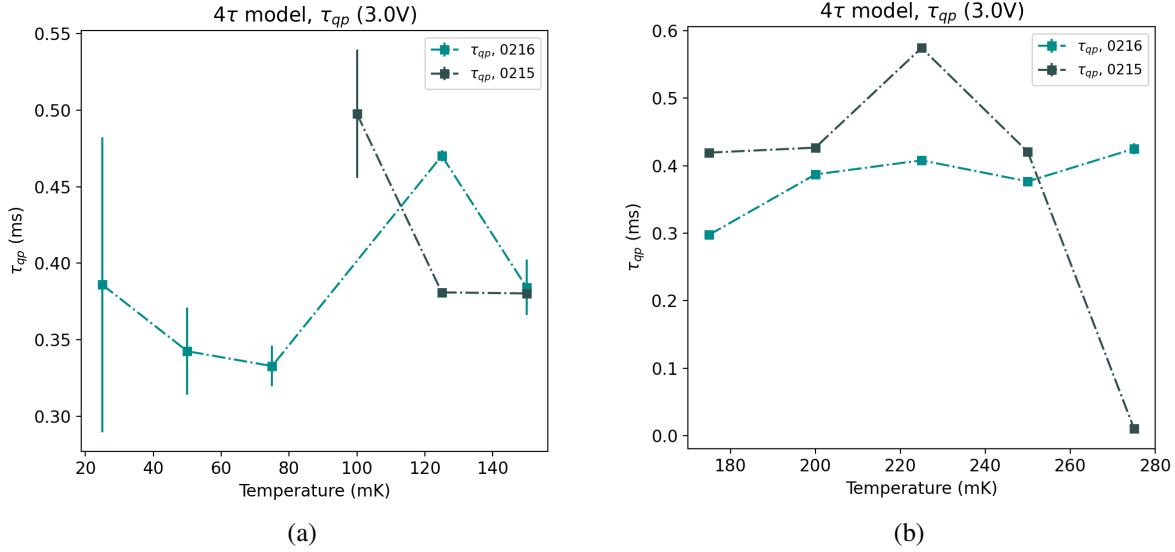


Figure 5.10: The 4 τ fit quasiparticle lifetime at (a) 25 mK to 150 mK and (b) 175 mK to 275 mK. Quasiparticle lifetime falls with increasing temperature, as expected, only at the lower temperatures. At high temperature the similarity between quasiparticle lifetime and delayed fall time suggested that they now serve the same function in the fit.

due to the increased quasiparticle density n_{qp} which increases with temperature. Physically, recombination of quasiparticle happens in higher density, leading to shorter lifetime. The data below 100 mK reflected this trend. At higher temperature, the trend goes the opposite of what current physics suggest, and the high uncertainty on the fall times invalidated the fit at the higher temperature. From 125 mK, we note that the trend in τ_{qp} and τ_{fp} are reversed, one increasing as the other decreases. Accordingly, τ_{qp} behaves similarly with τ_{fd} at high temperature (Fig. 5.9 (b), brown line; Fig. 5.10 (b), dark blue line). They functionally plays the same role. Potentially this could be explained by the derivation of the model from convolution: as τ_{qp} decreases, its convolution term gets significantly higher than that of the τ_{fd} term and dominates. The deviation from trends at higher temperature may suggested that the 4 τ model is not adequate to describe quasiparticle and phonon lifetimes at high temperature, but we cannot conclude definitively without first exhausts potential improvements in the fitting procedure.

5 τ model

Fig. 5.11 (top) shows the fall times at low and high temperature for 5 τ . The delayed fall time behaved as expected, decreasing with temperature until 125 mK and stays constant after. The prompt fall time's temperature-dependence at 75 mK and below is reversed, where it began at a magnitude lower than the empirical model and 4 τ predicts, then rise as temperature increases up to 75 mK before flattening again. Though this is unusual, the same trend is not replicated in the $V_{LED} = 4.0V$ dataset nor if we adjust the starting amplitudes of the fit. We note that in connecting

the lower and higher temperature regime, the delayed fall time forms a straight line at close to 1 ms, where the prompt fall time drops from around 1 ms to $\lesssim 0.6$ ms between 150 mK and 175 mK, rising up from 175 mK to 200 mK and fall again from 250 mK to 275 mK. The delayed rise times (bottom) is temperature-dependent from 25 mK to 100 mK, then fall from 1 ms to 0.01 ms at 125 mK. There is a spike in the delayed rise time at 175 mK; however, the high error bars suggested that this is a fit error, and the delayed rise time is largely temperature-independent, with a sudden drop between 100 mK and 125 mK.

The quasiparticle lifetime, as shown in Fig. 5.12, follows the expected temperature dependence. It decreases rapidly at lower temperature before the decreases slow down at 125 mK, finally falling to 0.0 at 200 mK and higher. In the reformatted equation as described in Sec. 4.3, where the 5τ model is the sum of a 3τ prompt and 4τ delayed component, a small τ_{qp} dominates the pulse by bringing other exponential term $\ll 1.0$, which may explains (or dominates) the unexpected behavior of the prompt fall time from 200 mK. We also see a correspondence between the delayed rise time behavior (Fig. 5.11 (b)) and the quasiparticle lifetime; since τ_{qp} is approximately half of τ_{rd} , the quasiparticle lifetime may dominate the delayed rise time at high temperature.

6 τ model

The 6 τ general temperature-dependence are, in general, much less insightful than the 4 τ and 5 τ case, in addition to having many more time constants with high error bars. Fig. 5.13 shows the fall and rise times of the 6 τ model at $V_{LED} = 4.0V$ data. Ignoring the data point at 225 mK and 275 mK (the delayed rise times there have high uncertainties), the delayed fall time follows the expected temperature dependence, flattening out at 75 mK, which is earlier than what the empirical model (150 mK), the 4 τ model (75 mK to 125 mK), the 5 τ (125 mK) predicted. At all temperature one of the time constants involved have extremely large uncertainty, and we see the same degeneracy behaviors between the prompt and delayed components that we saw in 4 τ at various points in Fig. 5.13: prompt and delayed rise time at 50 mK (bottom (a)), prompt and delayed fall time and rise time at 225 mK ((b)), and complete degeneracy of prompt and delayed rise time at 200 mK (bottom (b)). Particularly, at 200 mK, the prompt and fall rise time in 0216 is identical; the prompt rise time in 0215 dataset is also the same, without the delayed rise time being affected. This makes the 6 τ results uninformative with regard to the temperature-dependence of phonon lifetimes.

The quasiparticle lifetime in this model follows the expected temperature-dependence, where τ_{qp} decreases as temperature increases. Similar to 5 τ , at high temperature, τ_{qp} decreases more slowly. The quality of quasiparticle and phonon lifetimes in the 6 τ model is the inverse of what is shown in 4 τ : Here, τ_{qp} matches with known quasiparticle lifetime behaviors while phonon lifetimes fail; 4 τ model gives the expected phonon lifetimes behavior but not in the quasiparticle case. At high

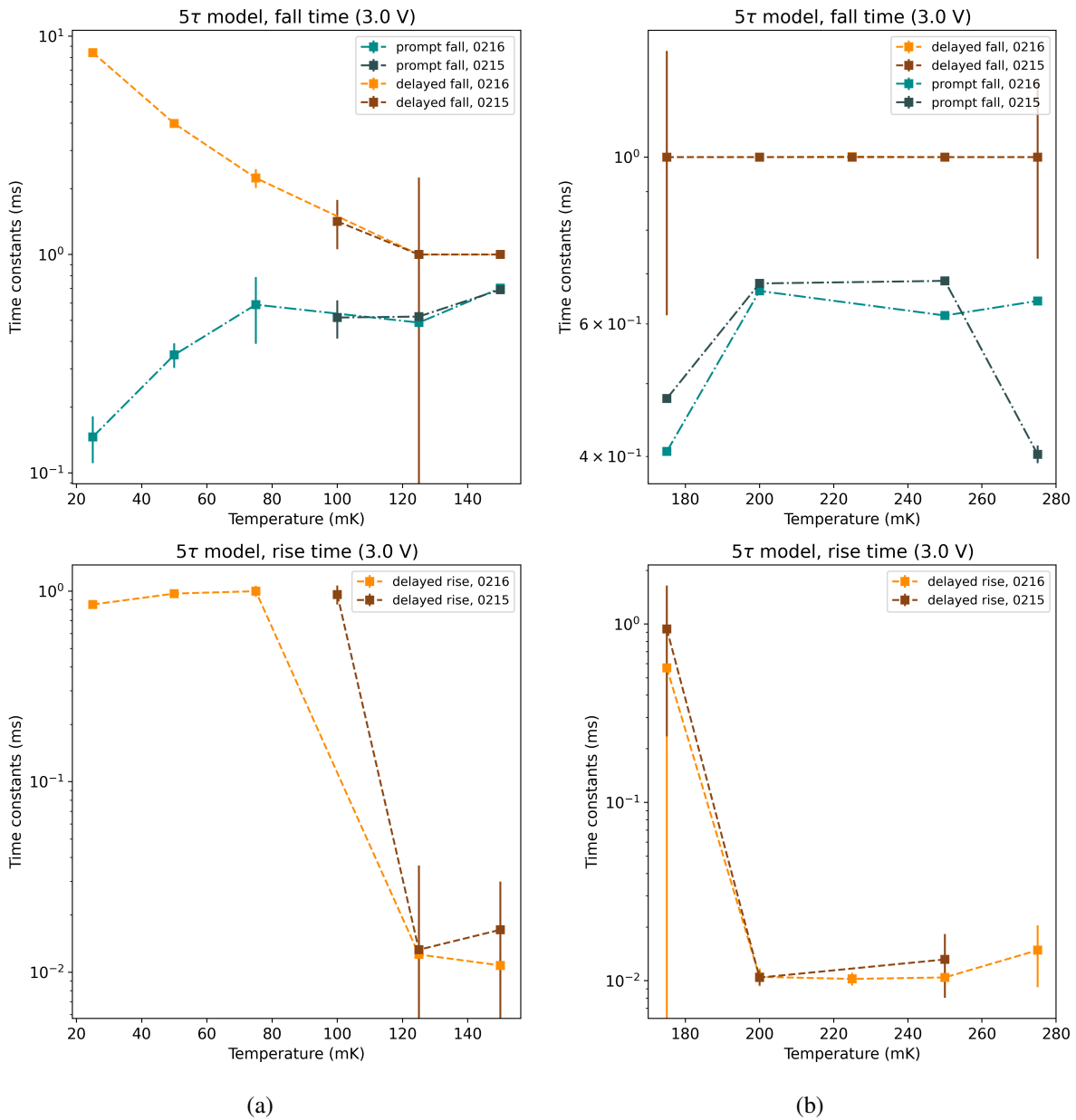


Figure 5.11: The 5τ fall times (top) and rise time (bottom) at (a) 25 mK to 150 mK, (b) 175 mK to 275 mK. The delayed fall time at both high and low temperature matches the empirical model's prediction. The prompt fall times reversed the expected trend and plummeted at high temperature, while the delayed fall time flattened as expected. The delayed rise time decrease from 75 mK to 125 mK then spiked at 175 mK. The high error bar there suggested that this is an outlier point, and the delayed rise time is temperature-independent at high temperature. The fall times agree between 0215 and 0216 datasets.

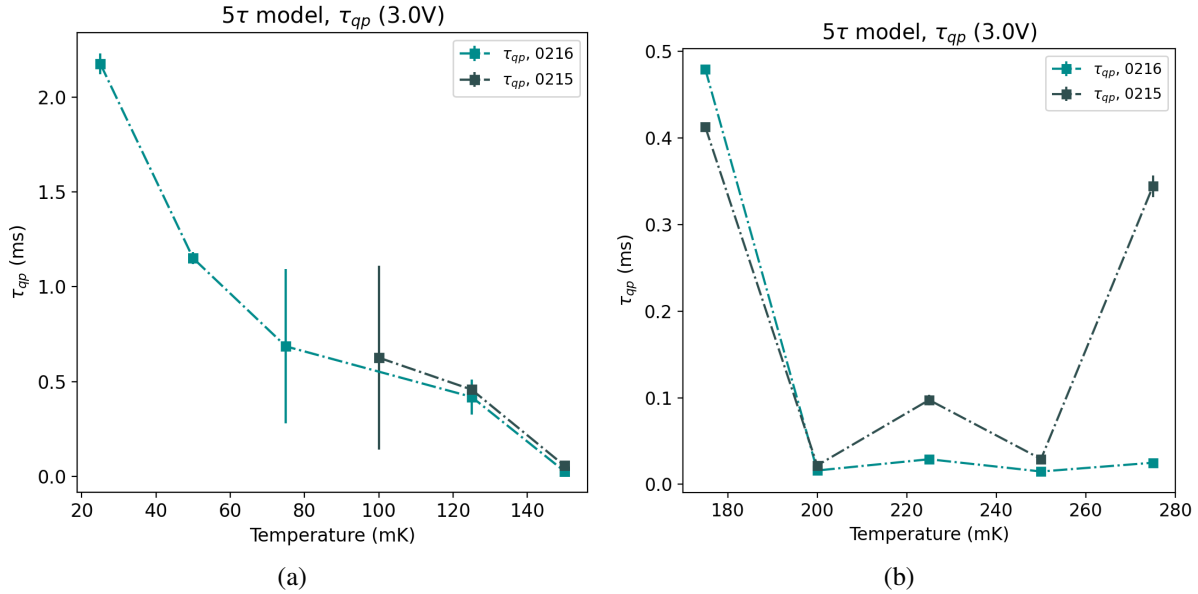


Figure 5.12: The 5τ quasiparticle lifetimes at (a) 25 mK to 150 mK and (b) 175 mK to 275 mK. Quasiparticle lifetime decreases with temperature in (a) as expected, falling down to 0.0 ms at high temperature.

temperature (175 mK and up), quasiparticle lifetime dominated the pulse; the phonon lifetimes is lost in the convolution, particularly the flattened delayed rise at 1 ms.

Comparisons

All in all, the 4τ model returned sensible phonon lifetimes temperature-dependence with inaccurate quasiparticle lifetimes behaviors; the situation is reversed in the 6τ model. The 5τ model, naturally as the compromise between the two models, has the expected quasiparticle lifetime behaviors and sensible phonon lifetimes. At low temperature, the prompt fall time has the reversed temperature-dependence compare to what is expected. However, this discrepancy is not reproduced by using a different dataset or by adjusting the starting amplitude of the fit. This, along with the time-dependence results, suggests that the 6τ models may have too many variables as the time constants become degenerate later on, and τ_{qp} dominates over those degenerate variables. The quasiparticle lifetimes in 4τ model suggests that it is also less accurate.

5.3 Amplitude- and Pulse width-dependence of fits

The difference in fits at different V_{LED} , as in Fig. 5.3, 5.2, 5.4 reveals that the fit quality is negatively affected by the increased LED voltage, which could specifically be due to the overall higher scaling of the data, resulting in higher amplitudes for a similar pulse width. We also observe this with fits at increasingly temperature, which shows that narrower curves are harder to fit for. Thus, there is a subtle amplitude-dependence and a stronger pulse width-dependence on the quality of the fit. This

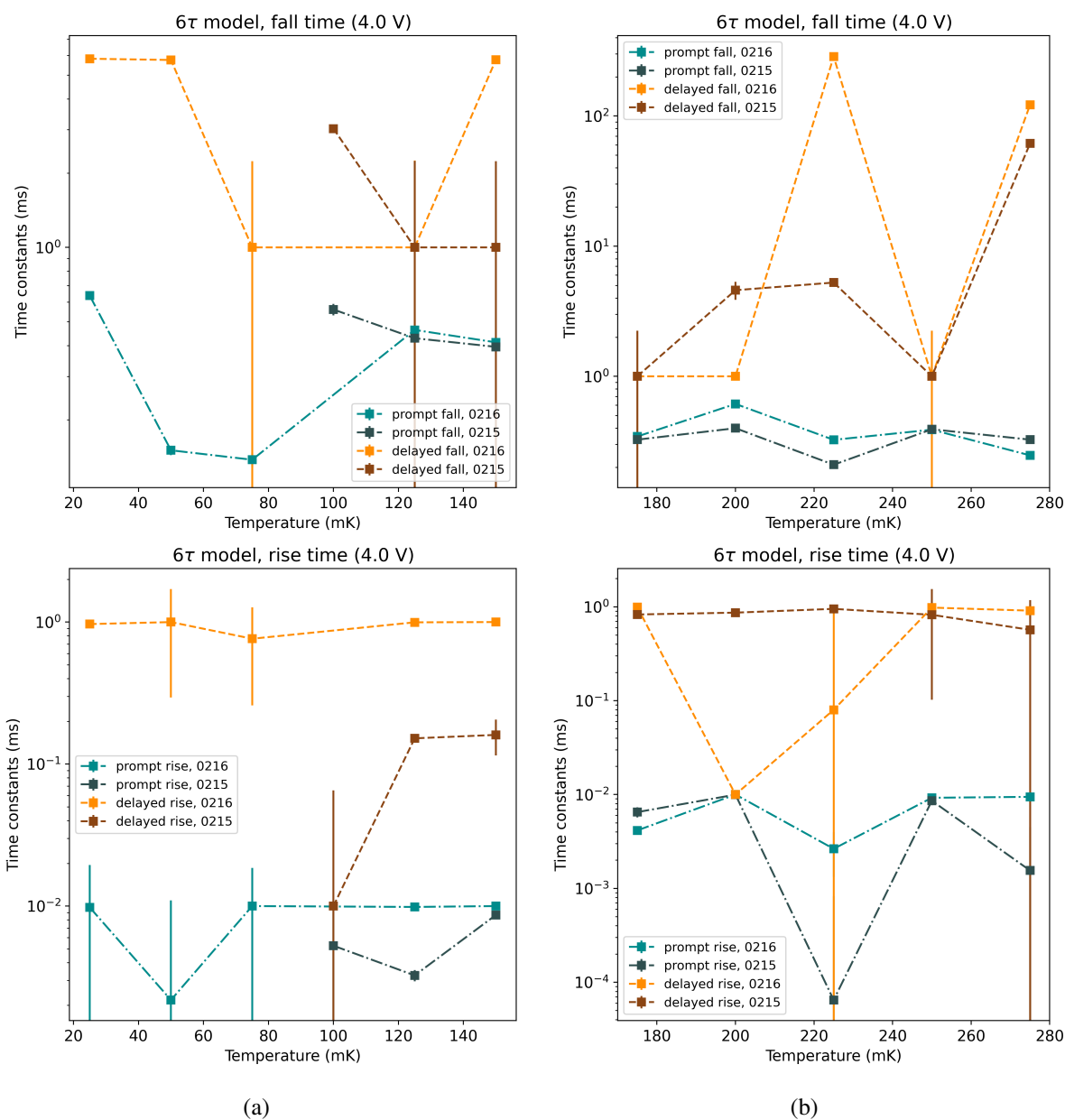


Figure 5.13: The 6τ fall times (top) and rise times (bottom) at (a) 25 mK to 150 mK, (b) 175 mK and 275 mK. Both prompt and delayed fall times fall steeply with temperature, as expected, at 25 mK to 75 mK. Accounting for the high error bars (i.e., ignoring the spike in delayed fall time at 225 mK and 275 mK (orange line)), we see delayed fall flats out at 75 mK. At 125 mK and higher, the prompt fall time follows the empirical model's trend of decreasing slightly with temperature. The rise times are affected by many fits degeneracy, thus are not informative.

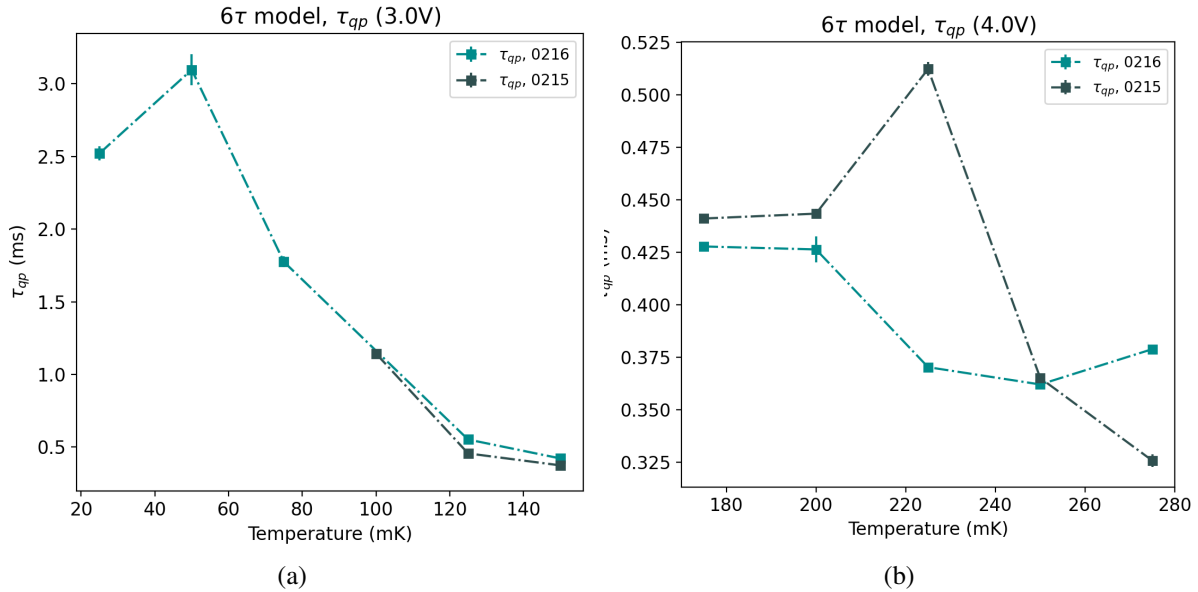


Figure 5.14: The 6τ quasiparticle lifetime at (a) 25 mK to 150 mK, (b) 175 mK to 275 mK. The quasiparticle lifetime decreases with temperature as expected through both low and high temperature regime. At high temperature, the quasiparticle lifetime decreases more slowly.

motivated the pruning of more early-time data at higher temperature for a better fit.

Comparison of different starting amplitude at high temperature

In Fig. 5.15, we plotted reduced χ^2 versus the starting amplitude, for the data at $V_{LED} = 4.0$. As the starting amplitude decreases for the same dataset, the reduced χ^2 also decreases, hinting at a better fit. At high temperature, most fits are relatively reasonable only at very low starting percentage. Notably, this is potentially a physically-relevant choice. We know that the quiescent quasiparticle density $n_{qp,0} \approx 20$ to $10\mu\text{m}^{-3}$ at lower temperatures. The convolution model, with the exponential shape, assumes $\delta n_{qp} \ll n_{qp,0}$ at some point in its derivation. The model is therefore most equipped to fit data below $n_{qp,0}$. However, $n_{qp,0}$ is not definitively known at higher temperature and could be much larger than $20\mu\text{m}^{-3}$. A lower reduced χ^2 does not always mean that the fit is better; due to the curve width issue at higher temperature (Fig. 5.8), decreasing the amplitude means matching the current fit to a wider part of the pulse. Particularly, at very high temperature where there are three apparent fall time constants (Fig. 4.1), starting later means excluding the very steep earlier time constants and focusing on the longer, later time constant, where the curve begins to widen as in Fig. 5.5. The very narrow pulse is thus excluded. However, drastic transitions in the reduced χ^2 typically marks a transition to a new fitted shape, as shown in Fig. 5.16.

Similarly, starting at a lower amplitude does not guarantee a better fit because there seems to be different regime where the fitted data either grossly overestimate the width of the pulse or not. As

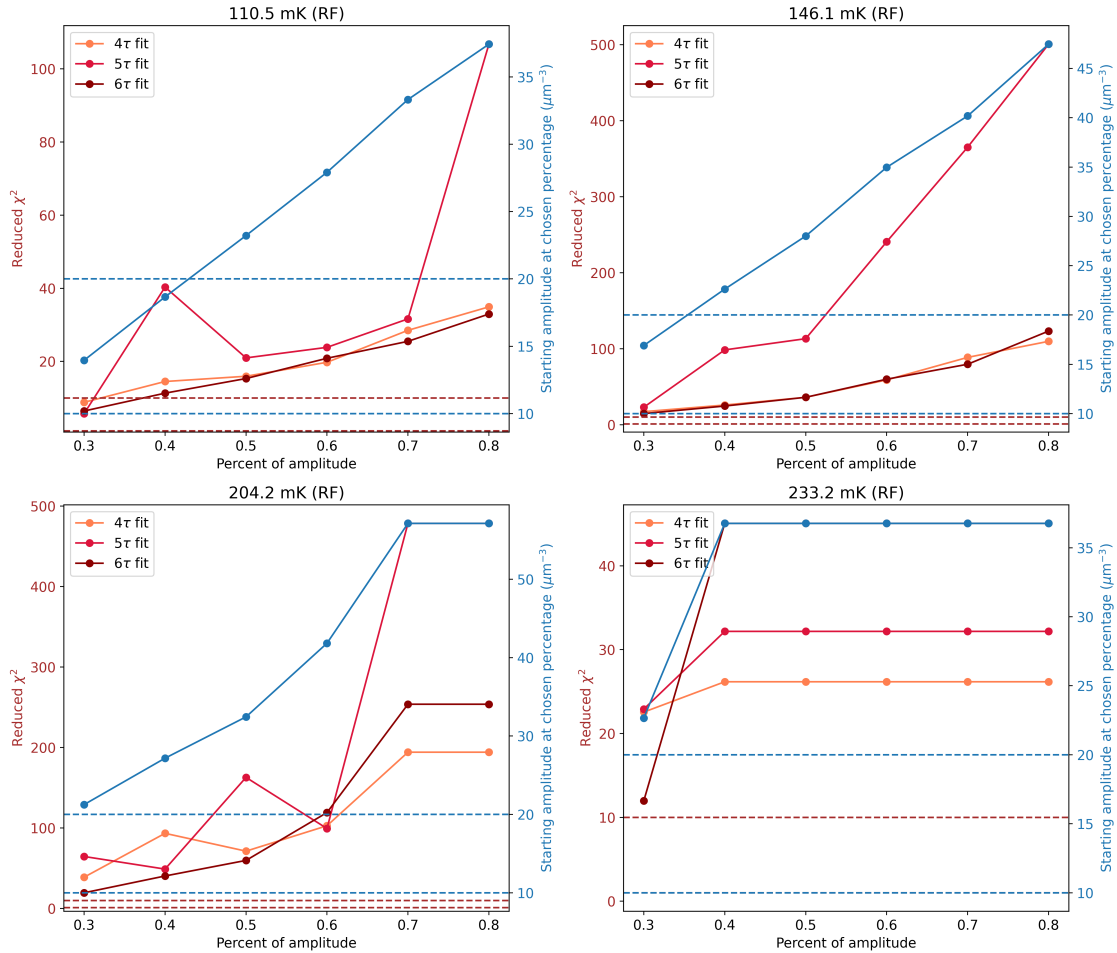


Figure 5.15: Plot of the reduced χ^2 (left, red) versus the starting amplitude (parameterized as the percentage of the true amplitude of the dataset), with the starting amplitude itself marked (right, blue). All three convolution models are plotted here. The dashed blue lines at $20\mu\text{m}^{-3}$ and $10\mu\text{m}^{-3}$ marked the expected range of the quiescent quasiparticle density at low temperature, though $n_{qp,0}$ may be much higher at high temperature. At all temperature, reduced χ^2 decreases as the starting amplitude chosen decreases. Top left: 125 mK. Top right: 150 mK. Bottom left: 225 mK. Bottom right: 300 mK. The flat lines present area where the closest point for the chosen starting amplitude is the same at different chosen percentage. This is especially common at higher temperature, where pulse falls very rapidly at earlier times.

referenced earlier by Fig. 5.4, occasionally, with appropriate starting condition, the fit can adapt to the narrower pulse. We see this in relation to the starting amplitude in the 175 mK, $V_{LED} = 3.0V$ data in Fig. 5.16, where the 5τ fit was able to return a reasonable fit at 80% starting amplitude, gets wider at 60%, and recovers the narrower fit at 30%. It is still unclear what is the cause outside of the starting amplitude. Further investigation is needed to determine if this is a reliable method of improving the fit.

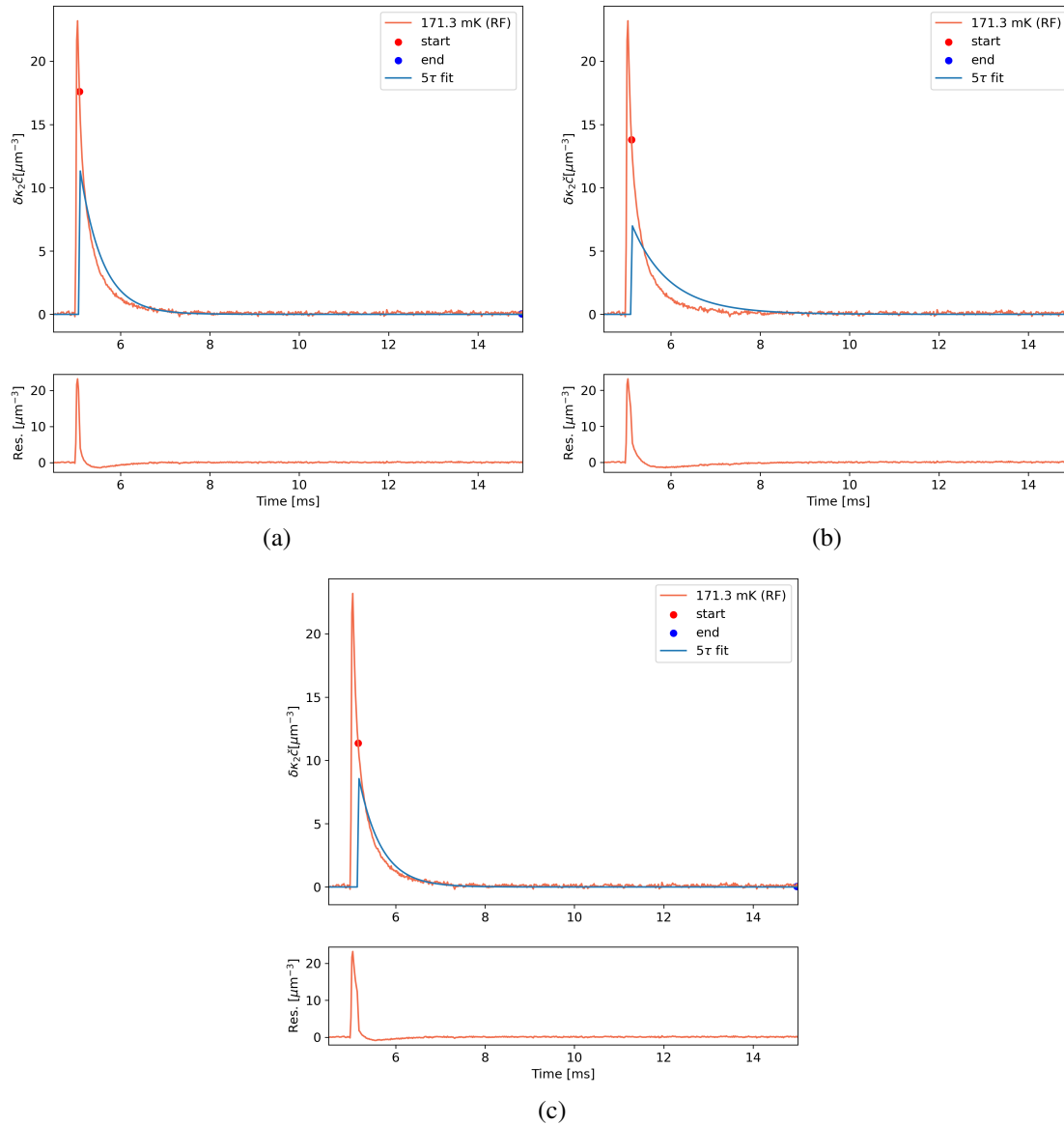


Figure 5.16: The 5τ fit at 175 mK and $V_{LED} = 3.0V$, at starting amplitude percentage (a) 80%, (b) 60 %, (c) 50%. Starting at lower amplitude does not always mean the fit will be better. There are different regime where the fitted pulse either grossly overestimate the width of the curve or not. The best reduced χ^2 returned is at 50%, emphasizing the point that for similar fitted pulse width, lower starting points simply improve χ^2 by excluding more data.

We referenced back to the time-dependence of time constants results for 5τ , where the prompt fall time temperature-dependence at 25 mK to 75 mK is seemingly reversed from what we expect, as demonstrated in Fig. 5.11. This trend is not replicated in any other choice of starting amplitude. Particularly, at 30% starting point, the original trend in this temperature range is restored, at the cost of the delayed fall temperature-dependence (Fig.5.17). This suggest that cutting out earlier rise and/or fall time, which 5τ model might (not) include, have an effect on whether the true temperature-dependence is revealed. Choosing the starting amplitudes, then, have a large effect on the quasiparticle and phonon lifetime that we are interested in, and we need to understand how the fits behave as we choose different time range for our data.

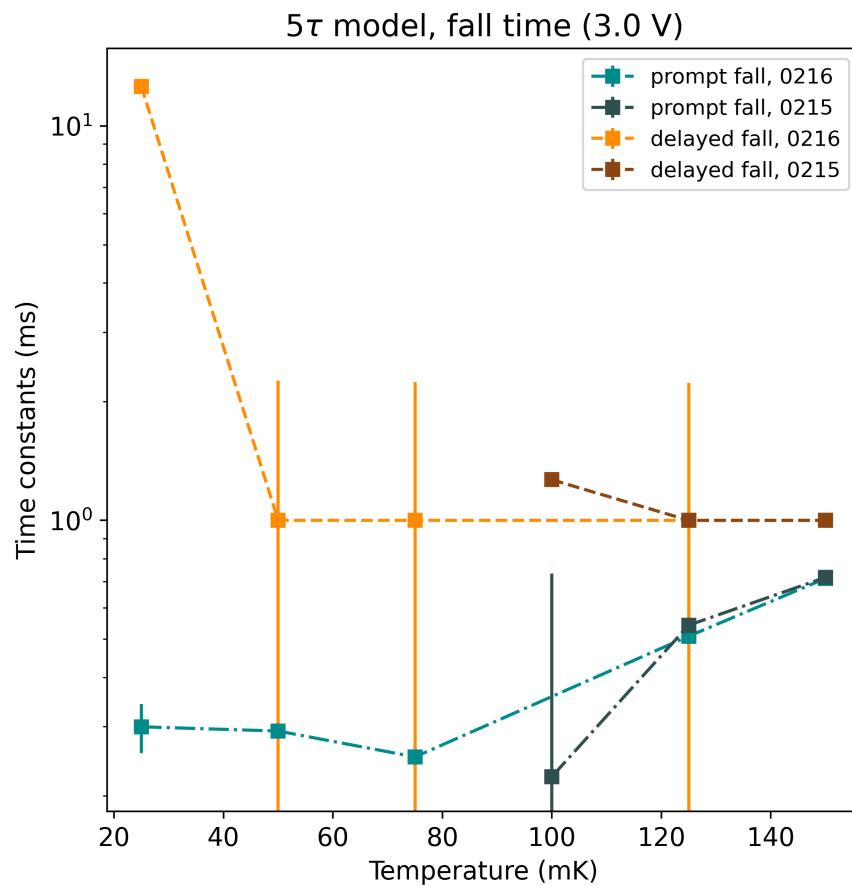


Figure 5.17: The 5τ temperature-dependence of prompt and delayed fall time from 25 mK to 150 mK, at starting amplitude 30%. We note here that compare to the data presented in 5.11, the 25 mK to 75 mK temperature-dependence is not reversed, and more closely resembles what we expect from the empirical fit.

Chapter 6

CONCLUSION

We are interested in formulating an accurate model for the pulse shape of the KIPM response, which is vital to obtaining an accurate energy resolution for the device. To this end, we formulated a physically-motivated model from quasiparticle and phonon lifetimes in the substrate, which necessitate understanding the evolution of these lifetimes at different temperature. The convolution models, with either six time constants (6τ), five (5τ), or four (4τ), are derived from the understood changes in quasiparticle density in the substrate and its thermalization to athermal phonon. The difference between each model is whether the delayed or prompt phonon rise time are included.

We obtained reasonably accurate fitting to all three models for low temperature data, from 25 mK to up to 125 mK in some cases, with high potential for improvement at higher temperature. We identified some challenges to the fitting procedure at high temperature, where higher amplitude and narrower pulses are difficult to fit, and we can potentially overcome this problem by avoiding to fit these portion of the curve, or, with further investigation, understand the condition that affect the width-dependence of the fit. Further investigation will also need to confirm whether this is a valid approach, though there is a potential physical motivation for this shifting of amplitude, particularly to where $\delta n_{qp} \ll n_{qp,0}$.

In terms of the goodness of fits between different models, all models fit approximately well at low temperature, with fit worsening at higher than 125 mK, though the 6τ model fits this higher temperature regime better than the 4τ or 5τ model. Examining the temperature-dependence of the lifetime constants reveal that 5τ returns the most sensible temperature-dependence for both quasiparticle and phonon lifetimes. This model predicted a similar temperature dependence to what is produced in the empirical model. On the other hand, the 4τ and 6τ model either returns a sensible phonon lifetimes or quasiparticle lifetime, respectively, as the other set of lifetime becomes unreliable. This indicates that the 5τ model is most suitable to fit the KIPM pulse shape, to be confirmed by an improvement in fitting technique and results, while the 4τ and 6τ models lead to a convoluted relation between quasiparticle and phonon lifetime by not having enough– or too many– floating variables.

6.1 Future work

Future work in refining the fitting procedure as well as the models presented are still needed, particularly in regard to higher temperature data. Proposed future directions, in regard to improving

the fit, include

- Investigating the relationship between pulse amplitude- and width- and goodness of fit.
- Understanding the variables affecting whether narrow pulse could be well-fitted or overestimated.
- Expand the analysis to more dataset, particularly at lower V_{LED} , to confirm the observations made here.

More minor changes can also be make, particularly in finding a more definitive criterion for the goodness of fit outside of the reduced χ^2 value. For example, the ratio between χ^2 (not reduced) value and degree of freedoms could be utilized, such that the goodness of fit is characterized as $\chi^2 = \alpha \sqrt{N_{DOF}}$, where $N_{DOF} = N_{points} - N_{params}$ is the degree of freedom, and a good fit would have $\alpha \sim 2$ to 3.

BIBLIOGRAPHY

- Aghanim, N. et al. (Sept. 2020). “Planck2018 results: VI. Cosmological parameters”. In: *Astronomy & Astrophysics* 641, A6. ISSN: 1432-0746. DOI: 10.1051/0004-6361/201833910. URL: <http://dx.doi.org/10.1051/0004-6361/201833910>.
- Bertone, Gianfranco and Dan Hooper (Oct. 2018). “History of dark matter”. In: *Rev. Mod. Phys.* 90 (4), p. 045002. DOI: 10.1103/RevModPhys.90.045002. URL: <https://link.aps.org/doi/10.1103/RevModPhys.90.045002>.
- Golwala, Sunil R (2000). “Exclusion limits on the WIMP nucleon elastic scattering cross-section from the Cryogenic Dark Matter Search”. PhD thesis. UC, Berkeley. DOI: 10.2172/1421437.
- Golwala, Sunil R. and Enectali Figueroa-Feliciano (2022). “Novel Quantum Sensors for Light Dark Matter and Neutrino Detection”. In: *Annual Review of Nuclear and Particle Science* 72, pp. 419–446. ISSN: 1545-4134. DOI: <https://doi.org/10.1146/annurev-nucl-102020-112133>. URL: <https://www.annualreviews.org/content/journals/10.1146/annurev-nucl-102020-112133>.
- Hans Dembinski, et al. (2022). *iminuit 2.31.1*. URL: <https://scikit-hep.org/iminuit/reference.html>.
- Hochberg, Yonit et al. (2016). “Detecting superlight dark matter with Fermi-degenerate materials”. In: *Journal of High Energy Physics* 2016 (8). DOI: 10.1007/JHEP08(2016)057.
- Markevitch, M. et al. (May 2004). “Direct Constraints on the Dark Matter Self-Interaction Cross Section from the Merging Galaxy Cluster 1E 0657–56”. In: *The Astrophysical Journal* 606.2, p. 819. DOI: 10.1086/383178. URL: <https://dx.doi.org/10.1086/383178>.
- Massey, Richard, Thomas Kitching, and Johan Richard (July 2010). “The dark matter of gravitational lensing”. In: *Reports on Progress in Physics* 73.8, p. 086901. DOI: 10.1088/0034-4885/73/8/086901. URL: <https://dx.doi.org/10.1088/0034-4885/73/8/086901>.
- Moore, David C (2012). “A Search for Low-Mass Dark Matter with the Cryogenic Dark Matter Search and the Development of Highly Multiplexed Phonon-Mediated Particle Detectors”. PhD thesis. California Institute of Technology. DOI: 10.7907/X8JD-4R90.
- Primack, Joel R. (Jan. 2017). “Cosmological Structure Formation”. In: *The Philosophy of Cosmology*, pp. 136–160. DOI: 10.1017/9781316535783.008.
- Sofue, Yoshiaki and Vera Rubin (2001). “Rotation Curves of Spiral Galaxies”. In: *Annual Review of Astronomy and Astrophysics* 39. Volume 39, 2001, pp. 137–174. ISSN: 1545-4282. DOI: <https://doi.org/10.1146/annurev.astro.39.1.137>. URL: <https://www.annualreviews.org/content/journals/10.1146/annurev.astro.39.1.137>.
- Strigari, Louis E. (Oct. 2013). “Galactic searches for dark matter”. In: *Physics Reports* 531.1, pp. 1–88. ISSN: 0370-1573. DOI: 10.1016/j.physrep.2013.05.004. URL: <http://dx.doi.org/10.1016/j.physrep.2013.05.004>.

Temples, Dylan J. et al. (Oct. 2024). “Performance of a phonon-mediated kinetic inductance detector at the NEXUS cryogenic facility”. In: *Phys. Rev. Appl.* 22 (4), p. 044045. DOI: 10.1103/PhysRevApplied.22.044045. URL: <https://link.aps.org/doi/10.1103/PhysRevApplied.22.044045>.

*Appendix A***RATIO BETWEEN PROMPT AND DELAYED AMPLITUDE**

Although not closely investigated in the duration of this project, we noticed an interesting effect where the amplitude of the delayed component of the fit may go to zero, thus became irrelevant, at low temperature, particularly in the case of $V_{LED} = 4.0V$, 6τ fit. Here a_s is the delayed (slow) fall time and a_f is the prompt (fast) fall time

